Diagnostic and prognostic value of cardiac magnetic resonance in patients with pulmonary hypertension

Lindholm, Anthony

2022

Document Version:
Förlagets slutgiltiga version

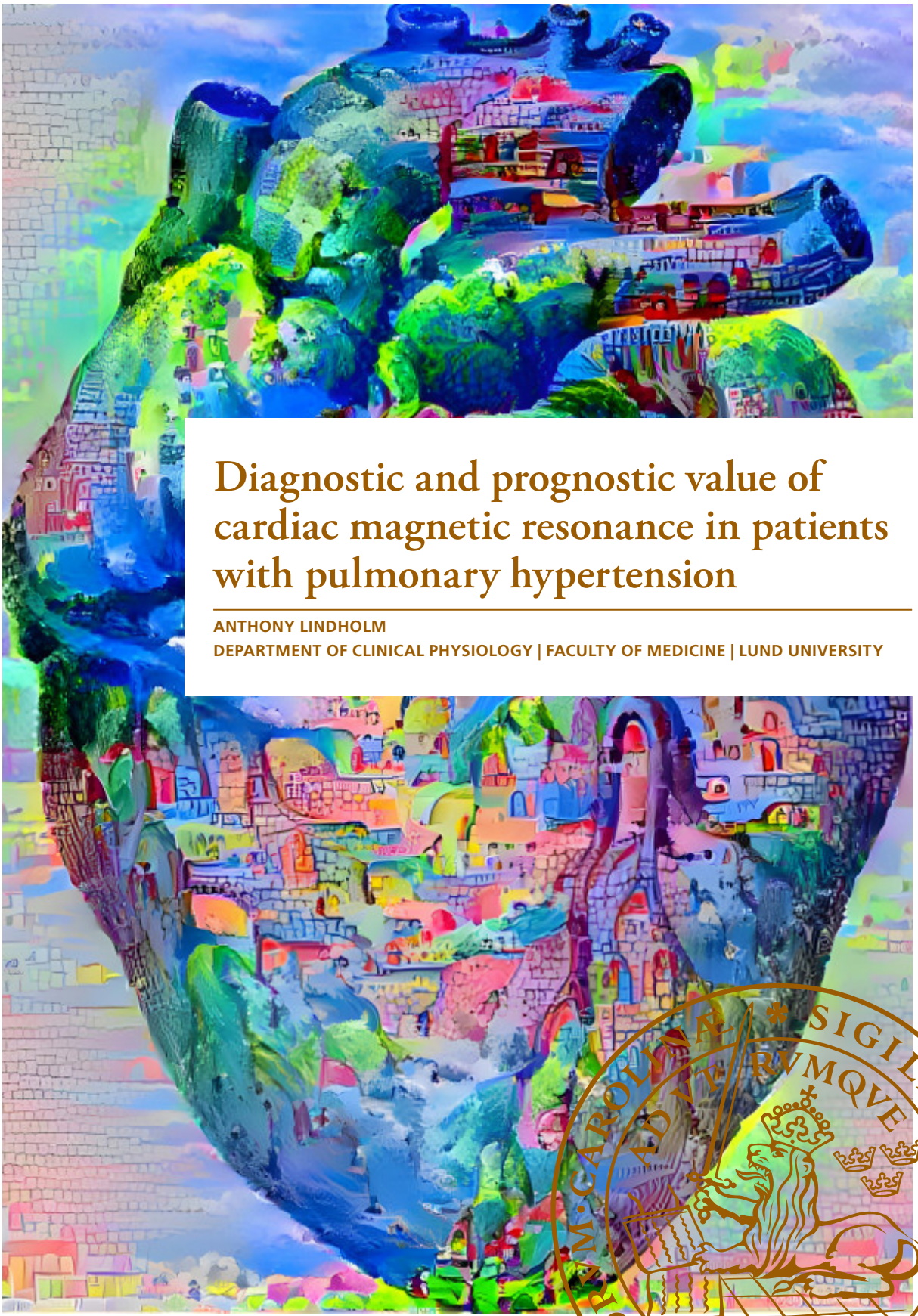

Diagnostic and prognostic value of cardiac magnetic resonance in patients with pulmonary hypertension

ANTHONY LINDHOLM
DEPARTMENT OF CLINICAL PHYSIOLOGY | FACULTY OF MEDICINE | LUND UNIVERSITY

Printed by Media-Tryck, Lund 2022 NORDIC SWAN ECOLABEL 3041 0903

LUND UNIVERSITY

FACULTY OF MEDICINE

Department of Clinical Physiology

Lund University, Faculty of Medicine
Doctoral Dissertation Series 2022:108
ISBN 978-91-8021-269-4
ISSN 1652-8220

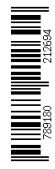

Diagnostic and prognostic value of cardiac magnetic resonance in patients with pulmonary hypertension

Diagnostic and prognostic value of cardiac magnetic resonance in patients with pulmonary hypertension

by Anthony Lindholm, MD

LUND
UNIVERSITY

Thesis for the degree of Doctor of Philosophy
Thesis advisors: Assoc. prof. Ellen Ostenfeld, Prof. Håkan Arheden, Assoc. prof. Göran Rådegran, Assoc. prof. Roger Hesselstrand
Faculty opponent: Prof. Anton Vonk Noordegraaf

To be presented, with the permission of the Faculty of medicine of Lund University, for public criticism in the lecture hall 3 (föreläsningssal 3) at the Skåne University Hospital, Entrégatan 7, Lund, Sweden on Thursday, the 8th of September 2022 at 13:00.

Organization
LUND UNIVERSITY
Department of Clinical Physiology
Entrégatan 7
SE–222 42 LUND
Sweden

Document name
DOCTORAL DISSERTATION

Date of disputation
2022-09-08

Sponsoring organization

Author(s)
Anthony Lindholm

Title and subtitle
Diagnostic and prognostic value of cardiac magnetic resonance in patients with pulmonary hypertension:

Abstract

Pulmonary arterial hypertension (PAH) is a rare disease with poor prognosis. The symptoms are often unspecific, which can lead to delayed diagnosis.
Cardiac magnetic resonance imaging (CMR) can be used to accurately assess the right ventricle (RV) and is the gold standard for measuring volumes and global ventricular function, such as ejection fraction. However, even with preserved ejection fraction subtle changes in cardiac function has been shown in patients with PAH.
Therefore, the aims for this thesis were to a) evaluate novel methods using CMR for early risk assessment of PAH, b) if these CMR measures are related to invasive measurements, and c) if CMR can assist improved prognostication.

The results of the publication where:
I. Lower biventricular longitudinal strain is mainly determined by increased pulmonary pressure and not by systemic sclerosis (SSc) per se. Low longitudinal strain are indicative of increased pulmonary arterial pressure and resistance.
II. Left ventricular (LV) longitudinal strain differed in SSc patients with insertion fibrosis or infarction compared to no fibrosis. SSc patients had lower RV longitudinal strain and strain rate compared to controls.
III. There was moderate to strong correlation of regional CMR measurements to corresponding echocardiographic measures such as RV lateral atrio-ventricular plane displacement (AVPD), maximum emptying velocity, RV fractional area change and RV free wall strain.
IV. Lower LV and RV AVPD were associated with increased risk for lung transplantation or mortality in patients with PAH.
V. Dyssynchrony measured as the standard deviation between time to peak strain and pulmonary valve closure from the six walls in three views (short axis, 4 chamber and RV 3 chamber) was associated with decreased transplantation free survival.

Key words
pulmonary arterial hypertension, cardiac magnetic resonance imaging, echocardiography, right ventricle, strain, atrioventricular plane displacement, regional contribution to stroke volume

Classification system and/or index terms (if any)

Supplementary bibliographical information

Language
English

ISSN and key title
ISSN: 1652-8220
Lund University, Faculty of Medicine Doctoral Dissertation Series 2022:108

ISBN
978-91-8021-269-4

Recipient's notes

Number of pages
181

Price

Security classification

Signature 

Date 2022-08-01

Diagnostic and prognostic value of cardiac magnetic resonance in patients with pulmonary hypertension

by Anthony Lindholm, MD

LUND
UNIVERSITY

A doctoral thesis at a university in Sweden takes either the form of a single, cohesive research study (monograph) or a summary of research papers (compilation thesis), which the doctoral student has written alone or together with one or several other author(s).

In the latter case, which is the form of the present thesis, the thesis consists of two parts. An introductory text puts the research work into context and summarizes the main points of the papers. Then, the research publications themselves are reproduced, together with a description of the individual contributions of the authors. The research papers may either have been already published or are manuscripts at various stages (in press, submitted, or in draft).

Cover illustration front: Building a little town in the heart. Created with https://deepdreamgenerator.com/

Faculty of medicine, Department of Clinical Physiology

ISBN: 978-91-8021-269-4

ISSN: 1652-8220
Lund University, Faculty of Medicine Doctoral Dissertation Series 2022:108

Printed in Sweden by Media-Tryck, Lund University, Lund 2022

There exists in such a case a certain institution or law; let us say, for the sake of simplicity, a fence or gate erected across a road. The more modern type of reformer goes gaily up to it and says, "I don't see the use of this; let us clear it away." To which the more intelligent type of reformer will do well to answer: "If you don't see the use of it, I certainly won't let you clear it away. Go away and think. Then, when you can come back and tell me that you do see the use of it, I may allow you to destroy it."

- G. K. Chesterton

Contents

List of publications

This thesis is based on the following studies, referred to by their Roman numerals:

I **Decreased biventricular longitudinal strain in patients with systemic sclerosis is mainly caused by pulmonary hypertension and not by systemic sclerosis per se**
A. Lindholm, R. Hesselstrand, G. Rådegran, H. Arheden, E. Ostenfeld
Clinical Physiology and Functional Imaging, 2019, 39(3), pp. 215–225

II **CMR feature tracking in cardiac asymptomatic systemic sclerosis: Clinical implications**
K. Bratis, **A. Lindholm**, R. Hesselstrand, H. Arheden, G. Karabela, E. Stavropoulos, G. Katsifis, G. Kolovou, G.D. Kitas, P.P. Sfikakis, L. Koutsogeorgopoulou, S. Mavrogeni, E. Ostenfeld
PLoS ONE, 2019, 14(8), e0221021

III **Right ventricular function parameters in pulmonary hypertension: echocardiography vs. cardiac magnetic resonance**
A.W. Evaldsson, **A. Lindholm**, R. Jumatate, A. Ingvarsson, G.J. Smith, J. Waktare, G. Rådegran, A. Roijer, C. Meurling, E. Ostenfeld
BMC Cardiovascular Disorders, 2020, 20(1), 259

IV **Atrioventricular plane displacement and regional function to predict outcome in pulmonary arterial hypertension**
A. Lindholm, B. Kjellström, F. Seemann, M. Carlsson, R. Hesselstrand, G. Rådegran, H. Arheden, E. Ostenfeld
International Journal of Cardiovascular Imaging, 2022

V **Right ventricular dyssynchrony predicts outcome in pulmonary arterial hypertension when assessed in multiple MR views**
A. Lindholm, B. Kjellström, G. Rådegrand, H. Arheden, E. Ostenfeld
Manuscript

Abbreviations

AVPD Atrioventricular plane displacement. 21–23, 35, 38, 46, 47, 49–52, 54, 55

CMR Cardiac magnetic resonance. 16, 25, 27, 30, 31, 35, 36, 38, 46–48, 51–55

CTEPH Chronic thromboembolic pulmonary hypertension. 9–11, 14, 51

EF Ejection fraction. 3, 6, 16, 19, 23, 27, 36, 47, 52–54

GLS Global longitudinal strain. 43–47, 50

LV Left ventricle. 1, 2, 6, 8–10, 16, 21, 23, 24, 27, 36–38, 43–46, 49, 50, 52, 53

mPAP Mean pulmonary arterial pressure. 4, 5, 10, 15, 43, 45, 52

PAH Pulmonary arterial hypertension. 5, 7–11, 13, 14, 16, 19, 27, 29, 30, 35, 36, 43, 44, 49, 51–55

PH Pulmonary hypertension. 4–6, 10, 13, 43, 49, 51

RHC Right heart catheterization. 9, 10, 16, 51, 53

RV Right ventricle. 1, 2, 7, 8, 11, 15, 16, 21, 24, 25, 27, 30–32, 34–39, 43–55

Acknowledgements

This has been a long and not always straight journey. It would not have been possible without the help, support and encouragement from my colleagues and family. This has only been possible due to teamwork, and I have been with a fantastic team.
I would like to thank the whole cardiac magnetic resonance group and the department of Clinical Physiology in Lund for giving me the opportunity to work, learn and develop for the last years. It has been a pleasure.
I would especially like to thank my supervisors. My main supervisor **Ellen Ostenfeld** for giving me the opportunity and guidance through this PhD. Thanks for your patience and for being available regardless of time. Thank you for helping me evolving my knowledge in research.
My co-supervisor **Håkan Arheden** for the conversations and reflections. Thank you for helping me in evolving my thinking both in work and in life. Thank you for holding the lecture in how the heart pumps in medical school. This was the foremost reason that I chose to go into research in cardiac magnetic resonance.
My co-supervisor **Göran Rådegran** for giving a clinical perspective. My co-supervisor **Roger Hesselstrand** for your enthusiasm and kindness. **Barbro Kjellström** for being more or less an extra supervisor. I have really learned a lot about writing and the scientific process from all of you. Thank you for the feedback.
I would like to thank **Katarina Steding Ehrenborg** for being the nicest and most helpful senior researcher possible when I started doing research in the cardiac MR group as a medical student. **David Nordlund** and **Per Arvidsson** for being helpful and kind when I was asking questions as a medical student attempting to do research. I try to pay it forward. **Erik Hedström**, **Anthony Aletras** and **Johannes Töger** for providing knowledge. **Einar Heiberg** and the rest of Medviso for always helping when needed.
I would also like to thank **Marcus Carlsson** and **Henrik Engblom** for the clinical education in cardiac magnetic resonance. The widened perspective and knowledge are invaluable. Thank you, Marcus, for asking questions that still make me think. **Henrik Mosén**, **Pia Sjöberg**, **Anders Nelsson**, **Johan Lundeberg** and **Bo Hedén** for the clinical education in clinical physiology.
Felicia Seemann, **Daniel Ryd**, **Björn Östenson** and **Anna Székely** for teaching me how to run the magnetic resonance scanner. **Felicia** for always being helpful when I was asking questions about the method of atrioventricular plane displacement and regional contribution, and for making changes to the code when necessary. **Jonathan Berg**, **Daniel Ryd**, **Petter Frieberg** for interesting discussions on cardiac physiology. **Mariam Al-Mashat** for always being helpful. **Karin Pola** and **Elsa Bergström** for the cooperation in pulmonary arterial hypertension. All my other fellow PhD students and senior researchers **Jonathan Edlund**, **Julius Åkesson**, **Jonas Liefke**, **Marjolein Piek**, **Kristian Dimovski**, **Tania Lala**, **Mikael Kanski**, **Robert Jablonowski**. Thank you for all the discussions and cooperation.

Jane Tufvesson for being helpful in the PhD process, and for always being present at the test presentations, providing valuable feedback.
To my co-authors outside of the Cardiac MR group, **Anna Werther Evaldsson** and **Konstantinos Bratis**. It was great working with you.
To the technologists including **Johanna M Koul**, **Charlotte Åkesson**, **Christel Carlander**, **Annmarie Svensson**, **Anna Sakaria**, **Ann-Helen Arvidsson** and **Reza Farazdaghi** for the clinical cooperation and for performing scans of the pulmonary arterial hypertension patients.
To my family.
My parents **Annette Lindholm Karlsson** and **Bertil Karlsson** for everything. My brother **Christoffer Lindholm** who has been working extra hard in my store, Unispel, to help me during the writing of this thesis. Thank you for helping with the dogs.
My son **Hugo Hiroki Nishimura Lindholm** for having patience while I have been working all day and night during the last part of my PhD. I hope we will be able to have some fun during the last part of the summer.
My fiancée **Mika Nishimura** for also having patience and for taking care of everything, including me, during the last part of this endeavor.

Popular summary in English

The circulatory system can be divided into two parts. One part originates in the right side of the heart and pumps blood to the lungs, the lung circulation. The other part originates from the left side of the heart and pumps blood to the rest of the body, the systemic circulation. Commonly, when talking about high blood pressure it is the pressure in the systemic circulation that is elevated.

Just as the blood pressure in the systemic circulation can be elevated, the blood pressure in the vessels of the lungs, the lung circulation can be elevated. High blood pressure in the lung circulation is very dangerous and can lead to that the right side of the heart no longer can pump blood and to early death. High blood pressure in the lung circulation is called pulmonary hypertension. It can be hard to arrive to a correct diagnosis as the symptoms can be quiet for a long time during the disease process. There can be many reasons for pulmonary hypertension. One especially serious reason for pulmonary hypertension is the disease systemic sclerosis.

Even with medical treatment pulmonary hypertension is a disorder with high mortality and only around 60% survives 5 years. To make the diagnosis and to select treatment for pulmonary hypertension there are many methods. For a definite diagnosis the pressure inside the heart is measured. This is done by inserting a pressure measuring device into the heart through one of the blood vessels in the body.

Before the pressure is measured in the heart patients with pulmonary hypertension are examined with echocardiography. The right side of the heart can be hard to visualize due to that the right side of the heart is concealed by the breastbone. It is also hard to calculate volumes in the right side of the heart due to its form. The volumes in the right side of the heart is easier to visualize and measure with cardiac magnetic resonance imaging.

The main aim of this thesis was to study how the function of the heart changes with pulmonary hypertension and systemic sclerosis with the aid of new methods with cardiac magnetic resonance imaging. The results of this thesis show that these new methods with cardiac magnetic resonance imaging can be used both for diagnosis for patients with pulmonary hypertension and systemic sclerosis. The results also show that these new methods with cardiac magnetic resonance imaging can be used for prognosis in patients with pulmonary hypertension. Finally we show that these new methods are comparable between echocardiography and cardiac magnetic resonance imaging, but that there are differences between the methods.

Populärvetenskaplig sammanfattning på svenska

Kroppens blodcirkulation kan delas upp i två delar. En del utgår från hjärtats högra sida och pumpar blod till lungorna, lungcirkulationen. Den andra delen utgår från hjärtats vänstra sida och pumpar blod till resten av kroppen, systemcirkulationen. När man i dagligt tal pratar om högt blodtryck menar man högt tryck i systemcirkulationen.

På samma sätt som man kan få högt blodtryck i systemcirkulationen kan man få högt blodtryck i lungornas kärl, lungcirkulationen. Att få högt blodtryck i lungcirkulationen är mycket farligt och kan leda till att hjärtats högersida inte längre orkar pumpa och därmed till för tidig död. Högt blodtryck i lungorna kallas för pulmonell hypertension. Det kan vara en svår diagnos att ställa då symptomen kan vara tysta långt in i sjukdomsförloppet. Det finns många orsaker till pulmonell hypertension. En orsak till speciellt allvarlig pulmonell hypertension är sjukdomen systemisk skleros.

Även med behandling med läkemedel är pulmonell hypertension en sjukdom som har hög dödlighet och endast ca 60 % överlever 5 år. För att diagnostisera pulmonell hypertension och för att välja behandling används flera metoder. För en definitiv diagnos måste man mäta trycket inne i hjärtat. Detta görs genom att en tryckmätare förs in i hjärtat via ett av kroppens blodkärl.

Innan man gör en tryckmätning undersöks patienter för pulmonell hypertension först med hjälp av ultraljud. Höger sida av hjärtat kan vara svårt att se med hjälp av ultraljud delvis på grund av att höger hjärthalva döljs bakom bröstbenet. Det är dessutom svårt att beräkna volymer på höger hjärthalva med ultraljud på grund av dess form. Höger hjärthalvas volymer är lättare att se och mäta med hjälp av magnetkameraundersökning.

Det övergripande syftet med denna avhandling var att studera hur hjärtats funktion förändras vid pulmonell hypertension och systemisk skleros med hjälp av nya metoder med magnetkameraundersökning. Resultaten i avhandlingen visar att dessa nya metoder med magnetkameraundersökning kan användas för diagnos både för patienter med pulmonell hypertension och systemisk skleros. Resultaten visar även att nya metoder med magnetkameraundersökning kan användas för att ställa prognos hos patienter med pulmonell hypertension. Till sist så visar vi att dessa nya metoder är jämförbara mellan ultraljud och magnetkameraundersökning, men att det också finns skillnader.

Part I

Research context

Chapter 1

1 Introduction

1.1 Cardiac anatomy and physiology

1.1.1 Cardiac anatomy

The heart is located in the middle of the chest between the lungs, behind and slightly to the left of the sternum [1]. It has four chambers. The upper chambers are called the left and right atria, and the lower chambers are called the left (LV) and right ventricles (RV) [1, 2]. The atria and ventricles are separated by the atrioventricular plane containing the mitral and tricuspid valves [3]. A wall of muscle and membrane called the septum separates the left and right sides of the heart [3, 4]. The LV is separated from the aorta by the aortic valve and the RV is separated from the pulmonary artery by the pulmonary valve [5] (Figure 1.1).

1.1.2 Cardiac physiology

If we follow the path of blood through the heart, deoxygenated blood returns to the right atrium from the lower body through the inferior vena cava and from the upper body through the superior vena cava [6]. The blood then passes from the right atrium to the RV through the tricuspid valve [6]. As the RV contracts and generates pressure, blood is ejected through the pulmonic valve, and enters the pulmonary artery [7]. The blood is thereafter transported through the pulmonary circulation where gas exchange occurs [8]. Blood returns to the left atrium, from the lungs, through the four pulmonary veins [9]. The blood then flows from the left atrium through the mitral valve, and into the LV [9]. When the LV contracts, blood is expelled through the aortic valve and into the aorta, which then distributes blood to the arterial system in the systemic circulation [10]. Finally, the blood returns to the right atrium and the cycle is repeated (Figure 1.2). The cardiac valves are structures that direct the blood flow in one direction and prevents reverse flow [11].

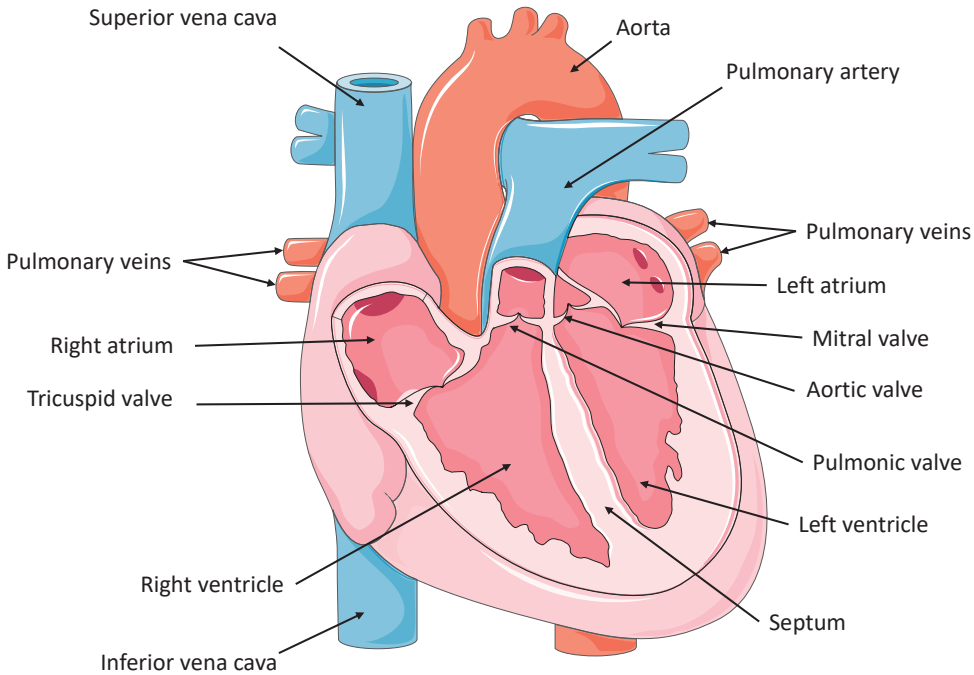

Figure 1.1: Schematic image of a normal heart with the right atrium in the upper left, the left atrium to the upper right, the right ventricle in the lower left and the left ventricle to the lower right. Adapted from smart.servier.com under Creative Commons Attribution 3.0 Unported License.

The atrioventricular valves open when the pressure in the atria is higher than in the ventricles and closes when the pressure is higher in the ventricles compared to the atria. The pulmonic valve opens when the pressure is higher in the RV compared to the pulmonary artery and the aortic valve opens when the pressure is higher in the LV compared to the aorta. When the pressure is higher in the opposite direction the valves close. This leads to blood only being transferred in one direction when the valves are healthy [11].

1.1.3 Cardiac cycle

In diastole the ventricles relax and are filled with blood [12]. Diastole can be divided into isovolumic relaxation, rapid inflow, diastasis and atrial systole [13]. The isovolumic relaxation starts when the pulmonary/aortic valves close and ends when the tricuspid/mitral valves open. Just as the name suggests there is no change in volume during this period. As the tricuspid/mitral valves open the ventricles are filled, first rapidly and then slowly in diastasis. After diastasis the atria contracts during atrial systole, further filling the ventricles.

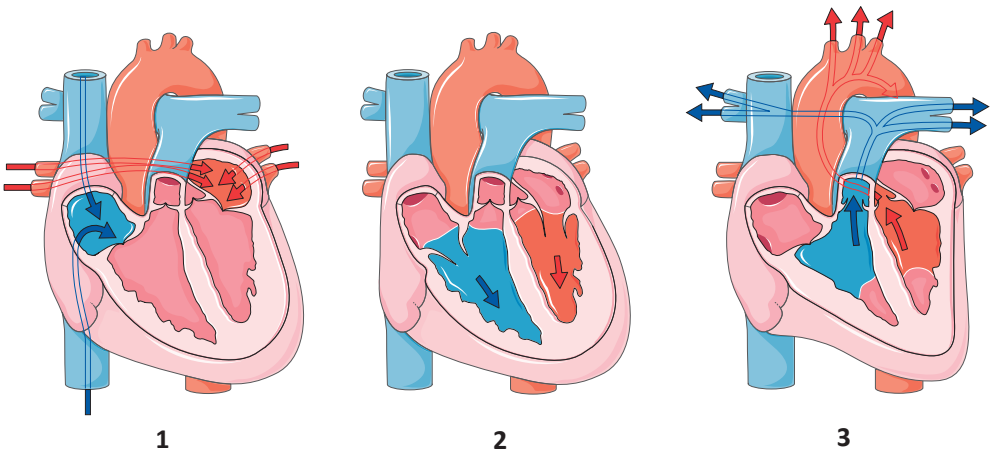

Figure 1.2: Schematic image of the heart cycle. 1. The blood returns to the right atrium via the inferior and superior vena cava and to the left atrium via the pulmonary veins. 2. Blood passes from the right and left atria to the right and left ventricles. 3. The ventricles contracts pushing the blood on the right side through the pulmonary artery to pulmonary circulation and the blood on the left side through the aorta to the systemic circulation. Adapted from smart.servier.com under Creative Commons Attribution 3.0 Unported License.

In the end of diastole, the ventricles are maximally filled, and this volume is called end diastolic volume. In systole the ventricles contract with ejection of the blood. Systole can be divided into isovolumic contraction and ejection [14]. The isovolumic contraction starts when the tricuspid/mitral valves close and ends when the pulmonary/aortic valves open. During this time there is contraction but no ejection. When the pulmonary/aortic valves open ejection starts and blood is ejected from the ventricles to the lungs and body. In the end of systole, the ventricles are minimally filled (maximally emptied) and is this volume is called end systolic volume. The difference between end diastolic volume and end systolic volume is called stroke volume. Stroke volume is the volume that is ejected with each heart stroke. Ejection fraction (EF) is defined as stroke volume divided by end diastolic volume and as such is a measurement of what fraction of the end diastolic volume is ejected with each contraction. The heart rate is the number of beats that the heart contracts with each minute. Cardiac output is the volume of blood that is ejected from the heart each minute and is calculated as stroke volume multiplied by heart rate [10]. The pressure is low on the right side of the heart due to a low resistance in the pulmonary circulation and high on the left side of the heart due to high resistance in the systemic circulation [15]. This results in thin myocardium on the right side and thick myocardium on the left side in the normal heart [16, 17].

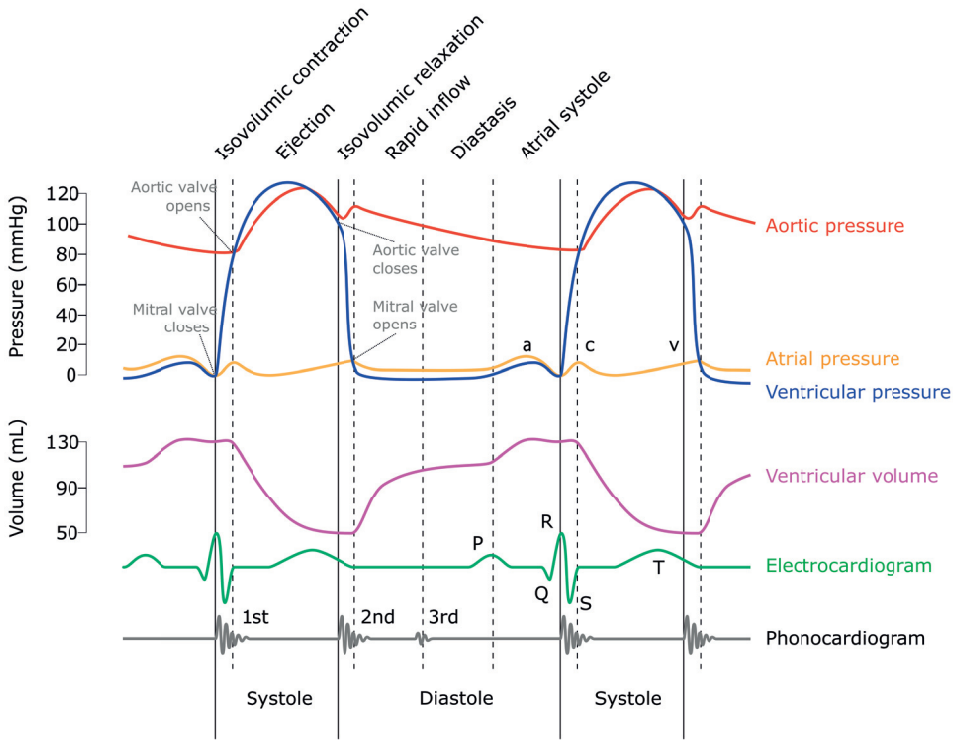

Figure 1.3: Wiggers diagram representing the cardiac cycle in the left ventricle. In the atrial pressure curve a) corresponds to the a-wave or the atrial contraction, c) corresponds to the c-wave due to the mitral valve bulging into the right atrium due to increased pressure in the left ventricle, while v) corresponds to the v-wave that corresponds to the rapid filling of the left atria. In the electrocardiogram the P-wave depicts the atrial depolarization, the QRS-complex the ventricular depolarization and the T-wave the ventricular repolarization. Reproduced from https://commons.wikimedia.org under CC BY-SA 4.0 license.

1.2 Pulmonary hypertension

1.2.1 Definition

Pulmonary hypertension (PH) is characterized by elevated blood pressure in the pulmonary circulation with mean pulmonary arterial pressure (mPAP) above 25 mmHg according to current ESC/ERS guidelines from 2015 [18]. It has been suggested by the "6th World Symposium on Pulmonary Hypertension task force" that this should be updated to mPAP above 20 mmHg [19, 20]. It can be expected that upcoming guidelines will change the limit to over 20 mmHg but for the studies in this thesis, we have used the current definition of above 25 mmHg.

PH can be subdivided by a hemodynamic definition into two broad subgroups of precapillary PH and postcapillary PH (Table 1.1). Precapillary PH has normal left atrial pressure

Table 1.1: Proposed hemodynamic definition of pulmonary hypertension.

Definition	Characteristics	Clinical groups
Pre-capillary PH	mPAP ≥20 mmHg PAWP ≤15 mmHg	1, 3, 4 and 5
Post-capillary PH	mPAP ≥20 mmHg PAWP <15 mmHg PVR 3 WU	2 and 5
Combined pre-capillary and post-capillary PH	mPAP ≥20 mmHg PAWP <15 mmHg PVR ≥3 WU	2 and 5

PH, pulmonary hypertension; mPAP,mean pulmonary arterial pressure; PAWP, pulmonary arterial wedge pressure; PVR, pulmonary vascular resistance; WU, Wood units. All values measured at rest. Adapted from European Respiratory Journal 2019 53 [12].

hence excluding PH caused by left sided cardiac disease. Postcapillary PH on the other hand has elevated left atrial pressure, due to left sided heart disease [18]. In addition, patients can have combined precapillary PH and postcapillary PH (Table 1.1). The left atrial pressure can be approximated by pulmonary arterial wedge pressure. [21].

PH can also be subdivided by clinical classification into five main groups: group 1: Pulmonary arterial hypertension PAH, group 2: PH due to left heart disease, group 3: PH due to lung diseases and/or hypoxia, group 4: PH due to pulmonary artery obstructions and group 5: PH with unclear and/or multifactorial mechanisms [19]. These groups can be further divided into subgroups (Table 1.2).
In the publications (1,2,4,5) for this thesis, we have focused on group 1 with the subgroups of idiopathic PAH, heritable PAH and PAH associated with connective tissue disease. With this in mind, the main focus of this thesis will be put on patients with PAH. In publication 3 we have also included patients from group 2, group 3 and group 4 (Table 1.2).

Table 1.2: Proposed clinical classification of pulmonary hypertension.

1 Pulmonary arterial hypertension
1.1 Idiopathic PH
1.2 Heritable PH
1.3 Drug- and toxin-induced PH
1.4 PH associated with:
1.4.1 Connective tissue disease
1.4.2 Human immunodeficiency virus (HIV) infection
1.4.3 Portal hypertension
1.4.4 Congenital heart disease
1.4.5 Schistosomiasis
1.5 PH long-term responders to calcium channel blockers
1.6 PH with overt features of venous/capillaries (PVOD/PCH) involvement
1.7 Persistent PH of the newborn syndrome
2 PH due to left heart disease
2.1 PH due to heart failure with preserved LVEF
2.2 PH due to heart failure with reduced LVEF
2.3 Valvular heart disease
2.4 Congenital/acquired cardiovascular conditions leading to post-capillary PH
3 PH due to lung diseases and/or hypoxia
3.1 Obstructive lung disease
3.2 Restrictive lung disease
3.3 Other lung disease with mixed restrictive/obstructive pattern
3.4 Hypoxia without lung disease
3.5 Developmental lung disorders
4 PH due to pulmonary artery obstructions
4.1 Chronic thromboembolic PH
4.2 Other pulmonary artery obstructions
5 PH with unclear and/or multifactorial mechanisms
5.1 Haematological disorders
5.2 Systemic and metabolic disorders
5.3 Others
5.4 Complex congenital heart disease

PH: pulmonary arterialhypertension; PVOD: pulmonary veno-occlusive disease; PCH: pulmonary capillaryhaemangiomatosis; LVEF: left ventricular ejection fraction; PH: pulmonaryhypertension.
Adapted from European Respiratory Journal 2019 53 [12].

1.2.2 Patophysiology

In PAH there is remodeling of pulmonary arteries, primarily in the arterioles [22]. The remodeling consists of endothelial dysfunction, proliferation of smooth muscle cells and proliferation of fibroblasts with increased extracellular matrix [23]. This leads to thickening of the pulmonary arteries [24]. Furthermore, there can be plexiform lesions and in situ thrombosis [25]. All of these changes lead to narrowing of the pulmonary arteries (Figure 1.4). [26, 27].

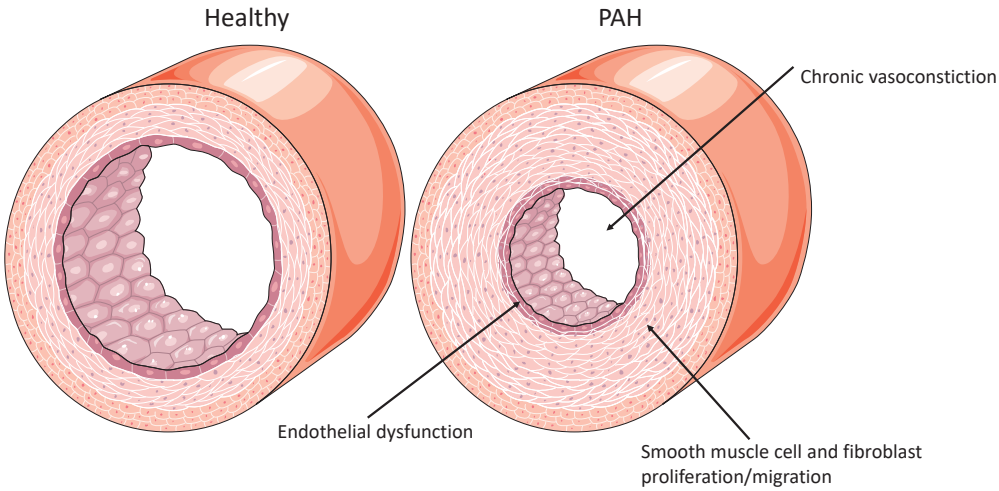

Figure 1.4: Schematic representation of the pulmonary arteries in pulmonary arterial hypertension (PAH) showing endothelial dysfunction, smooth muscle and fibroblast proliferation and migration as well as chronic vasoconstriction. Adapted from smart.servier.com.

The narrowing of the pulmonary arteries leads to increased resistance in the pulmonary vasculature. The increased pulmonary vascular resistance leads to increased RV afterload. The underlying mechanism behind the remodeling is a reduction in vasodilatory mediators such as prostaglandin I2, nitric oxide and cyclic guanosine monophosphate as well as increased endothelin and upregulation of endothelin receptors. These changes lead to vasoconstriction and proliferation [28]. Prostacyclin binds to the prostacyclin receptor and stimulates synthesis of cyclic adenosine monophosphate leading to vasodilation and antiproliferation in the pulmonary vasculature [31]. Nitric oxide stimulates soluble guanylate cyclase for synthesis of cyclic guanosine monophosphate which has vasodilatory and antiproliferative effects in the pulmonary vasculature [30]. Endothelin has vasoconstrictive and proliferative effect on the pulmonary arteries [29] (Figure 1.5).

The RV initially adapts to the increased afterload by increasing contractility leading to hypertrophy of the RV [32]. However, in the long run the RV dilates to maintain stroke volume with increased heart rate to maintain cardiac output. The dilation leads to in-

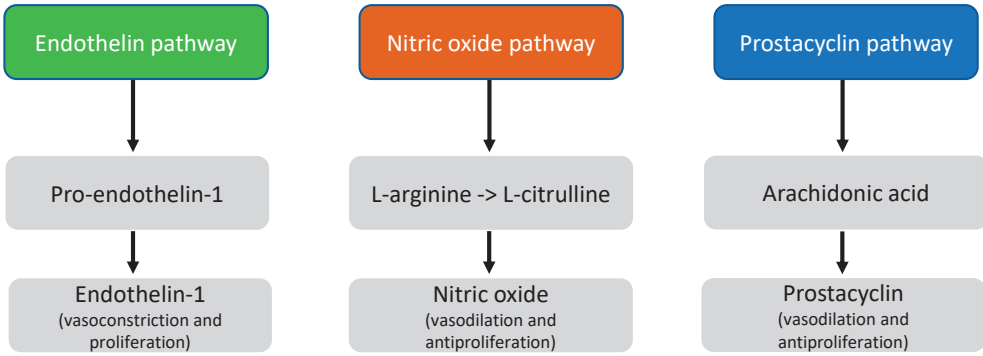

Figure 1.5: Schematic image of the mechanism behind vasoconstriction and proliferation in pulmonary arterial hypertension. Increased endothelin-1 leads to increased vasoconstriction and proliferation. Decreased nitric oxide and prostacyclin's leads to loss of vasodilation and antiproliferation.

creased wall stress that together with the RV hypertrophy and increased heart rate leads to increased oxygen demand (Figure 1.6). In the long term the RV is unable to compensate to the increased afterload which leads to RV failure (figure 1.7) [32, 33].

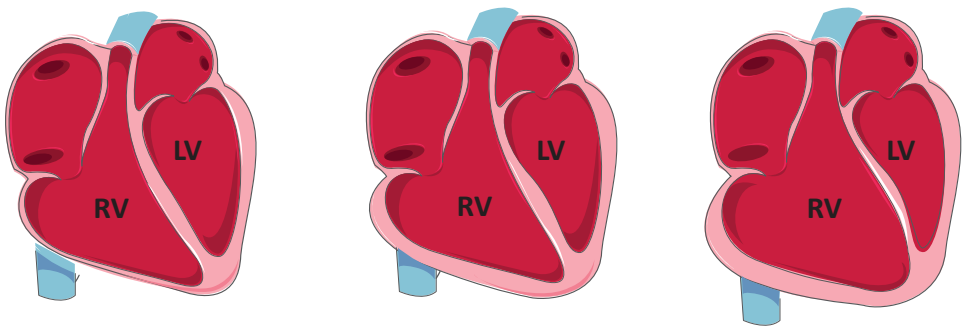

Figure 1.6: Schematic representation changes on the right ventricle (RV) due to increased afterload in patients with pulmonary arterial hypertension (PAH). In the normal heart (1) the right ventricular wall is much thinner compared to the left ventricular wall. In patients with PAH there is increased afterload and the RV adapts with hypertrophy (2). In an attempt to maintain stroke volume the RV dilates and the septum bows into the LV (3). Adapted from smart.servier.com.

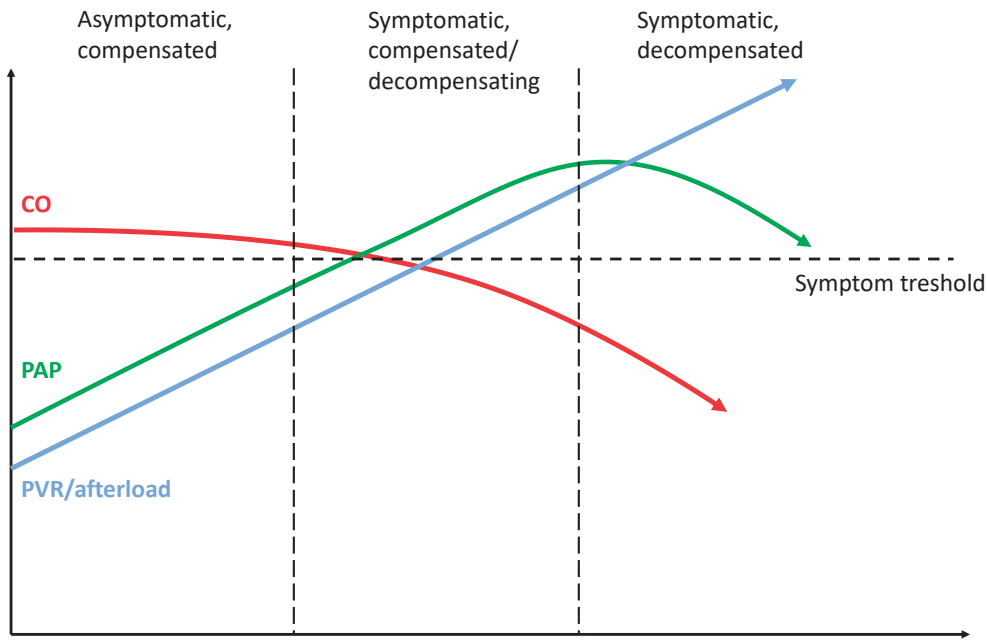

Figure 1.7: Schematic representation of the hemodynamic changes associated with disease progression in patients with pulmonary arterial hypertension. In the asymptomatic phase cardiac output is maintained while pulmonary artery pressure (PAP) and pulmonary vascular resistance (PVR) increases. In symptomatic, compensated/decompensating phase CO drops below the symptom threshold while both PAP and PVR is still increasing. In the symptomatic, decompensated phase CO drops further and the heart is no longer able to increase PAP while PVR increases. Adapted from European Heart Journal Supplements, Volume 9, Issue suppl_H, December 2007, Pages H68–H74 [34].

1.2.3 Symptoms and diagnosis

The early symptoms of PAH are unspecific and include fatigue, dyspnea, and decreased exercise capacity. Later symptoms such as chest pain and exertional syncope are also unspecific. The rarity of PAH in combination with the unspecific symptoms often leads to a delay in diagnosis [35–37].

After assessing the symptoms, and other signs that can be indicative of PAH, an echocardiography is commonly performed for initial assessment of the probability of PAH. If the echocardiography reveals high or intermediate risk for PAH, causes such as LV-disease and lung disease should be ruled out. To differentiate between chronic thromboembolic pulmonary hypertension (CTEPH) and PAH a ventilation/perfusion scan is performed. For both CTEPH and PAH a right heart catheterization (RHC) is performed for definite diagnosis. In CTEPH pulmonary angiography is also performed (Figure 1.8).

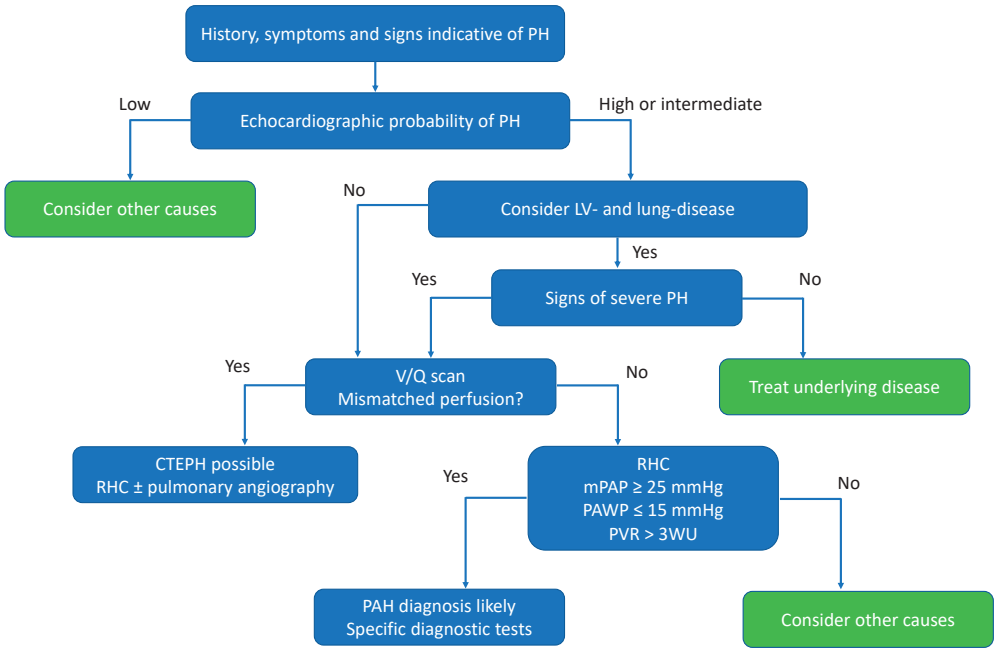

Figure 1.8: Simplified image of the diagnostic process for pulmonary hypertension. PH, pulmonary hypertension; LV, left ventricle; V/Q, ventilation/perfusion; RHC, right heart catheterization; CTEPH, chronic thromboembolic pulmonary hypertension mPAP, mean pulmonary arterial pressure; PAWP, pulmonary arterial wedge pressure; PVR, pulmonary vascular resistance; PAH, pulmonary arterial hypertension. Adapted from Eur Heart J. 2016 Jan 1;37(1):67–119[18].

1.2.4 Prognosis

The incidence of PAH is around 7 cases per million [38, 39]. Although there has been progress in the last decades with new therapy options, PAH is still a disorder with high morbidity and mortality rates [40–43]. Survival rate for PAH as a group is 85% - 87%, 67% - 73% and 57% - 65% respectively for 1-, 3- and 5-year survival rates [40–43]. In addition, the different etiologies of PAH have different mortality rates. PAH associated with connective tissue disease have worse prognosis compared to hereditary PAH and idiopathic PAH which have similar mortality [44, 45]. However, there is great difference in survival between PAH patients and it is important to diagnose the patients early and to have good prognostic makers for risk assessment. With early diagnosis and correct knowledge of disease severity and prognosis, treatment can increase survival (Figure 1.9).

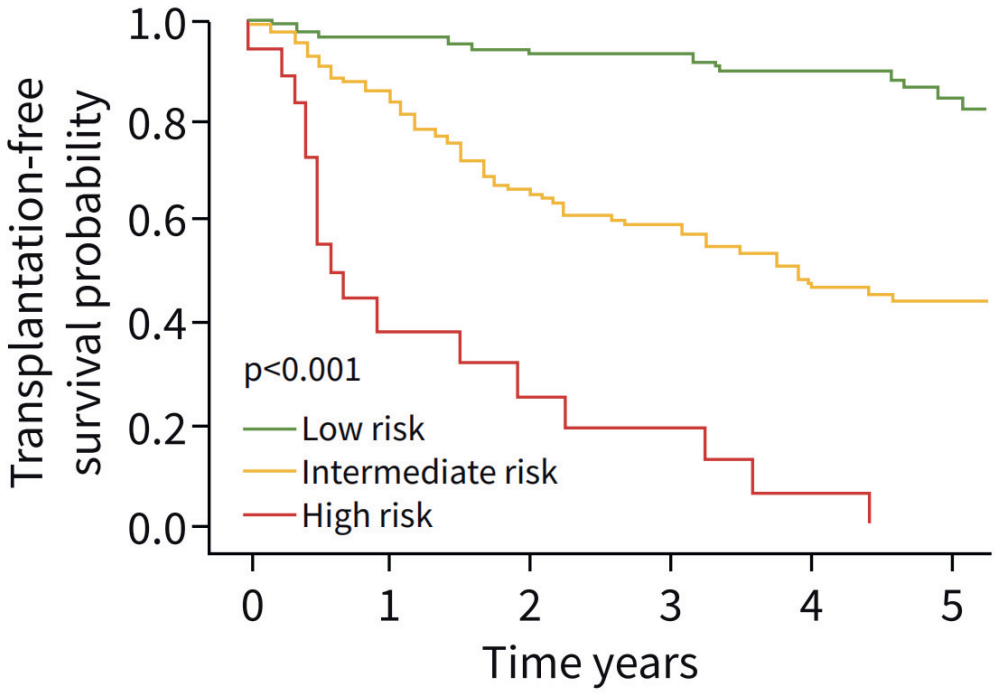

Figure 1.9: Transplant-free survival according to risk group at 3-year follow-up in patients with pulmonary arterial hypertension (PAH) from the Swedish PAH & CTEPH registry. The goal with PAH treatment is to lower symptoms and decrease mortality. It is important to improve diagnostic and prognostic methods for correct classification. Adapted from ERJ Open Res. 2021 Apr; 7(2): 00837-2020. [46]

1.2.5 Treatment

Current guideline treatment goals are to achieve a low-risk status of the patients focusing on exercise capacity, quality of life, RV function and mortality prognosis (Figure 1.9) [11]. There are three main pathways that are targeted with the currently approved specific PAH medications. These are the endothelin pathway, the nitric oxide pathway and the prostacyclin pathway, that all aim to reduce vasoconstriction and proliferation (Figure 1.10).

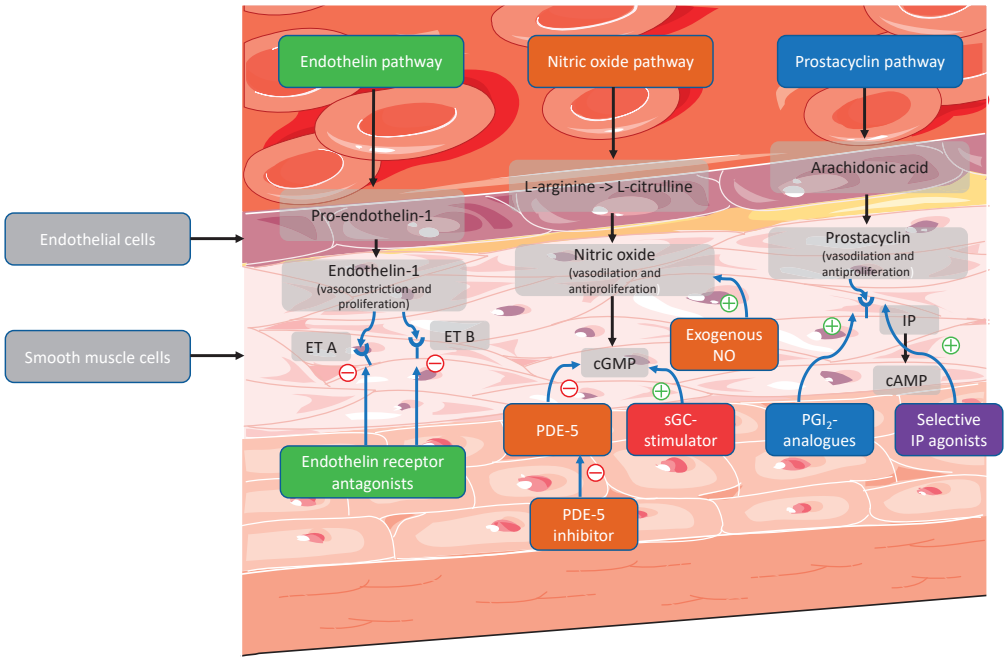

Figure 1.10: ET A, endothelin receptor A, ET B, endothelin receptor B; cGMP, cyclic guanosine monophosphate; NO, nitric oxide; PDE-5, phosphodiesterase type 5; sGC, soluble guanylate cyclase; IP, prostacyclin receptor; PGI2, prostacyclin; cAMP, cyclic adenosine monophosphate. Adapted from smart.servier.com.

Endothelin pathway: Endothelin receptor antagonists block the binding of endothelin to either both endothelin receptor A and B or selectively to receptor A. **Nitric oxide pathway:** Inhaled nitric oxide is not commonly used as a therapy but can be used as a rescue therapy. phosphodiesterase type-5 inhibitors leads to decreased cyclic guanosine monophosphate degradation by phosphodiesterase leading to higher concentration of nitric oxide [47]. Another way of increasing nitric oxide is by soluble guanylate cyclase-stimulators that increases the synthesis of cyclic guanosine monophosphate [48]. **Prostacyclin pathway:** Prostacyclin analogues as well as selective prostacyclin agonists binds to the prostacyclin receptor leading to vasodilation and antiproliferation. [18, 49]. In vasodilation responding patients calcium channel blockers can be used, leading to vasodilation [50].

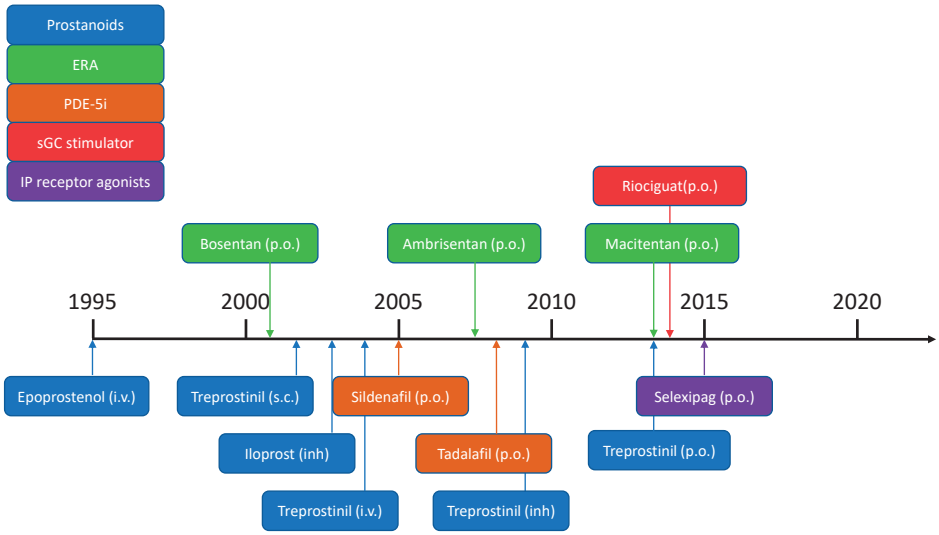

Figure 1.11: Timeline for approval of medications for pulmonary arterial hypertension based on the first date of approval in the EU or USA. ERA, endothelin receptor antagonist; PDE-5i, phosphodiesterase-5 inhibitor; sGC, soluble guanylate cyclase; IP, prostaglandin I2-receptor; i.v., intravenous; s.c., subcutaneous; p.o., oral; inh, inhalation. Adapted from European Respiratory Review 2017 26: 170095. [51]

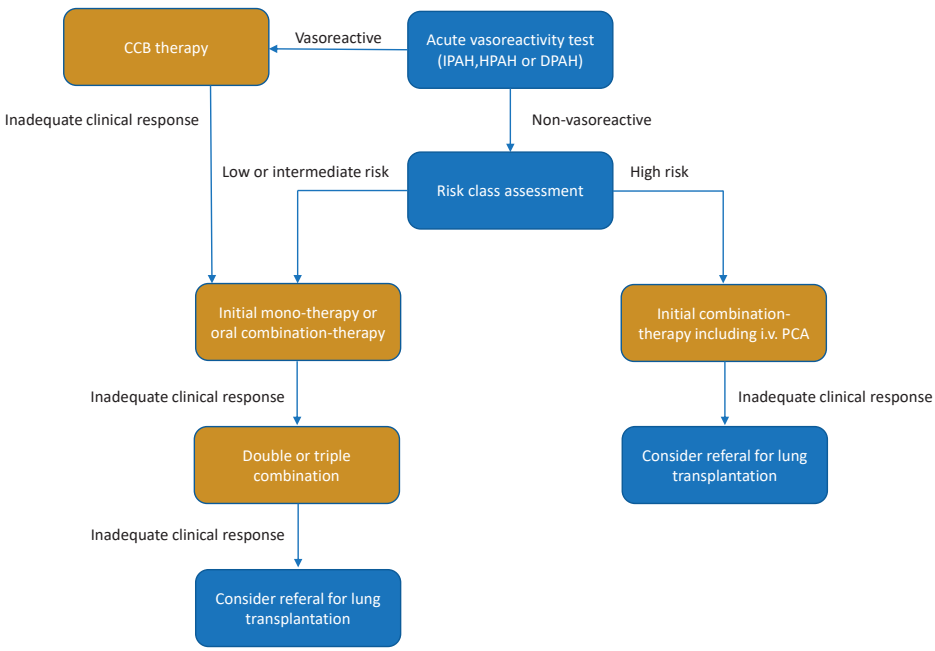

Figure 1.12: Simplified algorithm for treatment of pulmonary arterial hypertension (PAH). CCB, calcium channel blocker; IPAH, idiopathic PH; HPAH, hereditary PH; DPAH, drug induced PH; PCA, prostacyclin analogues. Adapted from European Respiratory Journal 2015. [18].

1.3 Systemic sclerosis

Systemic sclerosis is a rare connective tissue disease and even though there has been progress in the understanding of the disease the underlying pathogenesis is largely unknown. Mortality is still high with 2.7 times higher mortality in systemic sclerosis compared to the general population [52]. As PAH is one of the leading causes of morbidity and mortality in systemic sclerosis, patients with systemic sclerosis were included in the studies in this thesis [53]. The prevalence of systemic sclerosis is roughly 20 cases per million with a higher prevalence in women compared to men [54–56]. The main subtypes of systemic sclerosis are diffuse systemic sclerosis and limited systemic sclerosis, where diffuse systemic sclerosis has mean survival of around 10 years, and limited systemic sclerosis 30 years [54]. The latest classification criteria are based on skin phenomena such as skin thickening and Raynauds phenomena, abnormal nailfold capillaries, PAH and systemic sclerosis related antibodies (Table 1.3) [57]. The criteria were updated in 2013 by ACR and the European League Against Rheumatism (EULAR) [57].

Table 1.3: 2013 classification criteria for systemic sclerosis. The criteria are not applicable to patients with skin thickening sparing the fingers or to patients who have a scleroderma-like disorder that better explains their manifestations.

Item	Sub-item(s)	Score[a]
Skin thickening of the fingers of both hands extending proximal to the metacarpophalangeal joints *(sufficient criterion)*	–	9
Skin thickening of the fingers *(only count the higher score)*	Puffy fingers	2
	Sclerodactyly of the fingers (distal to the metacarpophalangeal joints but proximal to the proximal interphalangeal joints)	4
Fingertip lesions *(only count the higher score)*	Digital tip ulcers	2
	Fingertip pitting scars	3
Telangiectasia	–	2
Abnormal nailfold capillaries	–	2
Pulmonary arterial hypertension and/or interstitial lung disease *(maximum score is 2)*	Pulmonary arterial hypertension	2
	Interstitial lung disease	2
Raynaud's phenomenon	–	3
SSc-related autoantibodies (anticentromere, anti–topoisomerase I [anti–Scl-70], anti–RNA polymerase III) *(maximum score is 3)*	Anticentromere Anti–topoisomerase I Anti–RNA polymerase III	3

2013 classification criteria for systemic sclerosis: an American collegeof rheumatology/ European league against rheumatism collaborative initiative. [a],the total score is determined by adding the maximum weight (score) in each category. Patients with a total score of ≥9 are classified as having definiteSSc. Reprinted with permission from BMJ Publishing Group Ltd. Ann Rheum Dis.2013.[57].

1.4 Right heart catheterization

Right heart catheterization is gold standard for hemodynamic assessment and is required for diagnosis of PAH and CTEPH according to current guidelines [18, 58]. During the procedure right atrial pressures, right ventricular pressures, pulmonary arterial pressures,

pulmonary arterial wedge pressures as well as cardiac output are measured [59, 60]. Pulmonay vascular resistance is calculated as mPAP minus mean pulmonary artery wedge pressure divided by cardiac output. Right heart catheterization is an invasive method but when performed in expert centers the morbidity and mortality are low with around 0.3% procedures leading to hospitalization and 0.06% to fatalities [61]. The procedure is usually done under local anesthesia. The venous system is most commonly accessed through the femoral vein, brachial vein or the internal jugular vein [62–64]. This can be done with or without ultrasound guidance [65]. A Swan-Ganz catheter has a balloon added to the catheter tip allowing placement in the heart by flotation with the cardiac flow [60]. The Swan-Ganz catheter also has a thermistor enabling measurement of temperature as well as a proximal port for injection of saline [66]. The placement of the catheter can be monitored with fluoroscopy but can also be monitored by analyzing the waveforms. Around 20 cm from the internal jugular vein the right atrium is reached and the pulsatile atrial waveform is seen (Figure 1.13). After the right atrial pressures has been measured the catheter is further advanced to the RV and the right ventricular waveform is acquired. Thereafter the pulmonary wedge pressure is usually measured by advancing the catheter to the wedge position. Finally the catheter is retracted to the pulmonary artery and the pulmonary arterial pressures can be obtained (Figure 1.13).

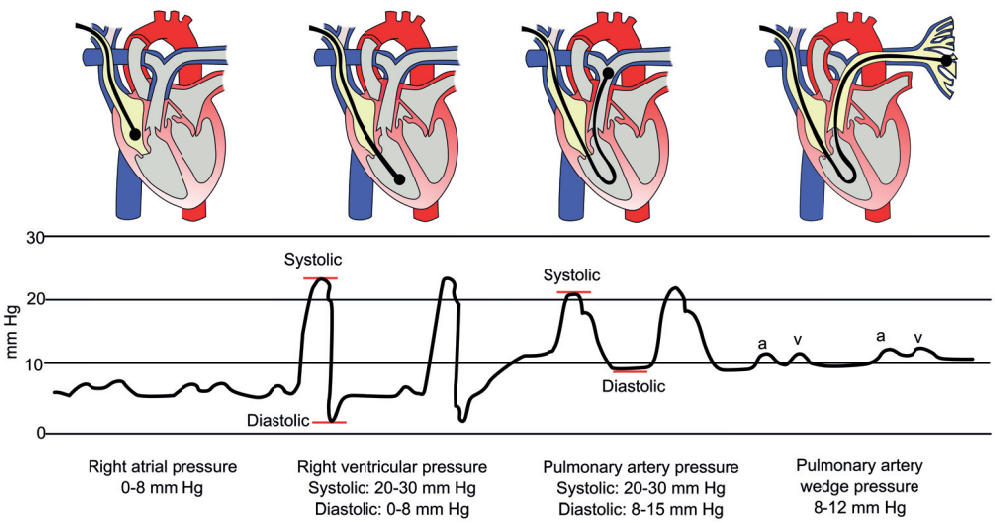

Figure 1.13: Schematic image of right heart catheterization in a subject without pulmonary arterial hypertension. Pulsatile pressure waveforms are measured in A: the right atrium, B: the right ventricle, C: the pulmonary artery and D: the pulmonary artery wedge. Reprinted from pcipedia.org, licensed under Creative Commons Attribution-NonCommercial-ShareAlike.

While the catheter is placed with the thermistor in the pulmonary artery cold saline is injected into the right atrium via a proximal port. By measuring the drop in temperature

with the thermistor while the blood moves from the right atrium to the pulmonary artery, cardiac output can be calculated [66].

1.5 Echocardiography

Detection of PAH is currently performed with transthoracic echocardiography as first-line non-invasive method [67]. Besides looking at morphology, pericardial effusion and standard echocardiographic measures, including LVEF, right sided estimates are performed [67]. Echocardiography uses ultrasound with frequencies between 2 to 5 MHz for adults and up to 12 MHz for children, well over audible frequencies between (20Hz to 20 kHz) [68]. The ultrasound frequencies are generated with an ultrasound probe with piezo-electric crystals [69]. Some of the ultrasound waves are reflected, especially when at the interfaces between different tissue densities. When the probe detects the returning waves, or echoes, it can process the information and display it as moving images. Simplified there are three main modes of imaging, 1. 2D echocardiography imaging represents the echoes as bright dots composing a 2-dimensional image [68], 2. M-mode imaging provides a 1-dimensional view with the benefit of higher temporal resolution [70, 71], and 3. Doppler imaging that estimates the velocity of the blood flow [72, 73]. Apart from evaluation of cardiac function, echocardiography can be used to approximate pulmonary pressure by measuring peak velocity of the tricuspid regurgitation [74, 75]. This makes echocardiography a mainstay in the diagnosis in PAH. This difference in pressures between the RV and right atrium are calculated by assessment of jet peak velocity of tricuspid valve regurgitation using the Bernoulli equation [74]. The pressures obtained with this method correlates well with invasive measures of systolic pulmonary arterial pressures with RHC [75].
Global RV function is notoriously a challenge to assess with echocardiography when compared to cardiac magnetic resonance imaging (CMR). [76]. The LV can be geometrically modelled like an ellipsoid and thereby volumetric data can be mathematically approximated from long axis images. However, the shape of the RV is complex with outspread in- and outflow tract, crescent shape and is highly trabeculated which greatly complicates volumetric RV measurements by echocardiography [77, 78].

1.6 Cardiac magnetic resonance imaging

CMR offers an alternative method of measuring volumes and function in the heart and is considered the reference standard for assessing RV anatomy, volumes and function [76, 79]. Volumes and function with CMR correlates with outcome in PAH and could be used to monitor therapy effect [80–83]. In addition CMR can with high accuracy and reproducibility assess flow in the cardiac vessels such as the pulmonary artery [79]. However, CMR is still not fully implemented in standard care in PAH and the availability of CMR

is variable around the world and is only scarcely available in developing countries [76, 84, 85].

1.6.1 Generation of the magnetic resonance signal

The magnetic resonance scanner consists of four main parts to generate and receive the magnetic resonance signal. The first part is the static magnetic field that is, in most cases, generated by a superconducting magnet [86]. This field, B_0, is generated in the direction of the bore, or in the z-direction. The second part is the radiofrequency coils used to generate radiofrequency pulses in order to flip the magnetic field in the direction perpendicular to the bore, B_1, or the x-y-direction [87]. The third part are the gradient coils that can create magnetic gradients that vary linearly in all three directions, x-y-z [88]. Finally, to receive the magnetic resonance signal there are receiver coils [89]. The primary origin of the magnetic resonance signal used to generate most clinical images comes from the abundance of water in the body, containing two hydrogen nuclei [90]. Hydrogen nuclei consist of a single proton that carries a positive electrical charge, and these protons generates a magnetic dipole [91].

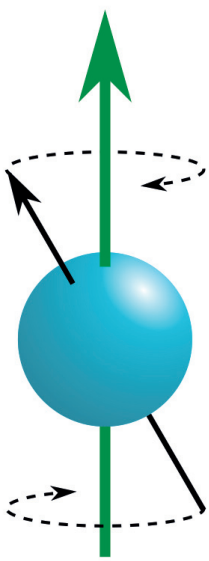

Figure 1.14: Schematic image of the precessing motion of a proton in an external magnetic field. Reprinted from commons.wikimedia.org, Creative Commons Attribution-No Rights Reserved license.

The magnetic field for each proton is known as a magnetic moment. The magnetic moments for these protons are normally randomly orientated. However, when an external magnetic field B_0 is applied there will be a bias in the number of protons that precess around an axel aligned either with (parallel) or against (antiparallel) the external field [92]. The parallel direction is a lower energy state compared to the antiparallel direction and the spins align according to the Boltzmann distribution [93]. In room temperature this means

that slightly more spins precess towards the parallel direction ant that there will be a net magnetization in the direction of B_0.

The rate of precession will occur at the Lamor frequency, ω, which is dependent on the strength of the magnetic field B_0 and the gyromagnetic ratio γ.
Larmor frequency: $\omega = B_0 \times \gamma$ [94].
The Larmor equation indicates that precession frequency is proportional to the strength of the magnetic field. The gyromagnetic ratio for hydrogen is approximately 42,6 MHz per Tesla and with a field strength of 1.5 Tesla the Larmor frequency is approximately 64 MHz.

The next step is to apply a radiofrequency pulse, with the same frequency as the Lamor frequency. This will lead to two effects. One effect is that the bias in the parallel direction will decrease resulting in lower net magnetization in the z-direction. The second effect is that the protons will precess in phase. This results in a transverse magnetization vector rotating with the Lamor frequency in the x-y-plane. Since the transverse magnetization vector is spinning in the x-y-plane it is an oscillating magnetic field, generating an electric current. Therefore, a conductive receiver coil can receive the resulting electrical current. When the radiofrequency pulse stops there is a loss off phase as well as a return to the lower parallel energy state. This is the relaxation of the magnetic resonance signal.

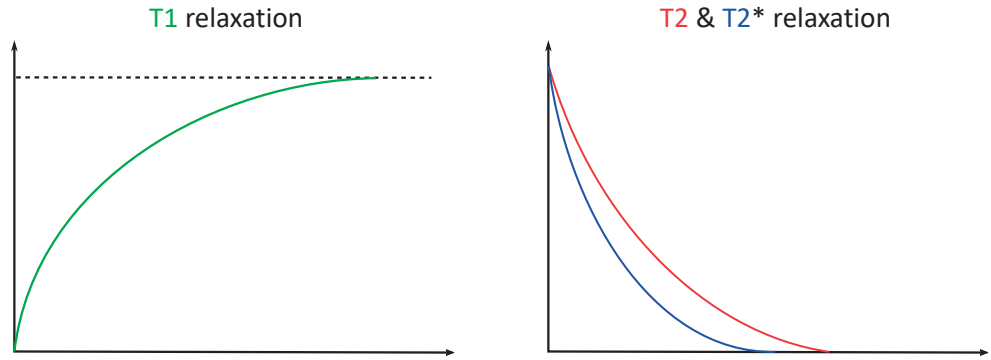

Figure 1.15: T1, T2 and T2* relaxation with 90° flip angle. After the radiofrequency pulse has been applied the magnetization vector will flip from the z direction to the xy-direction. The magnetization in z-direction will increase over time due to spin-lattice interactions, called the T1 relaxation in green. Likewise, the magnetization in xy direction will decrease, due to spin-spin interactions, called T2 relaxation, in red, or in reality rather due to spin-sin interactions and inhomogeneities in the magnetic field, T2* relaxation, in blue.

This relaxation can be divided into T1-relaxation due to spin-lattice interactions and T2-relaxation because of dephasing due to spin-spin interactions. T1-relaxation is the recovery of longitudinal magnetization, in z-direction. The T2-relaxation is the decline in transversal magnetization, in x-y-direction. In reality the transversal relaxation will decrease both due to spin-spin interactions and inhomogeneities in the magnetic field called T2* relaxation. T1-relaxation is a slower process and T2-relaxation is a faster process. T1- and T2-relaxation times are different in different tissues and is one of the main principles in

which contrasts are created in magnetic resonance images.

1.6.2 Spatial encoding

The signal is encoded in three dimensions by using the gradient coils creating small linear magnetic gradients in three dimensions.

Slice selection

To be able to perform slice selection a slice selection gradient is applied before the radiofrequency pulse is applied. This creates a gradient field in the z-direction where the protons will have slightly different Larmor frequencies. When the radiofrequency pulse is applied only the spins that corresponds to that specific frequency will flip. As the radiofrequency pulse is sent as a small range of frequencies, protons will flip with slightly different Larmor frequencies. In this way we will not receive a strictly 2-dimensional slice but rather a slice with a specific slice thickness that depends on the width of the frequency range applied by the radiofrequency pulse.

Phase encoding and frequency encoding

After slice selection we have to decipher the signal in the x-y direction. To be able to do that we will apply phase and frequency encoding gradients. After the radiofrequency pulse has been applied the protons will precess in phase with each other with the same frequency. When the phase gradient is applied the frequency of the spins will be different, depending on the position within the phase gradient. When the phase gradient is turned off the protons will return to having the same frequency but with the spins being out of phase. The difference in phase will be linearly dependent on localization within the gradient. This will provide an opportunity to decipher the location of the signal in the phase direction. The frequency encoding gradient is applied perpendicular to the phase encoding gradient during readout and will cause the protons to spin at different frequencies. The frequency gradient will not be turned off as the phase gradient and thus the frequencies of the spins will be different for different protons. The frequency of the spins will vary in a linear manner depending on the frequency gradient.

1.7 Regional function

Measuring cardiac function is essential for diagnosis and prognosis in many heart diseases. The most common way of measuring cardiac function is global function with for example EF and stroke volume. Volumes and global function correlates with outcome in PAH [80–83]. Stroke volume and EF are results of myocardial shortening. Regional function are

more closely related to describing the myocardial shortening and leads to deeper understanding of the pump physiology of the heart.

1.8 Strain

One method of assessing regional function is myocardial strain. Strain is the relative geometrical change, or deformation, of the myocardium during the cardiac cycle. This change is measured in three directions in the heart, longitudinal, circumferential and radial [95]. By measuring the length of the myocardium in the longitudinal direction through the heart cycle the change in longitudinal strain can be appreciated [95]. By comparing longitudinal length measured in end diastole and end systole we will get the relative longitudinal shortening of the myocardium, or longitudinal systolic strain (Figure 1.16).

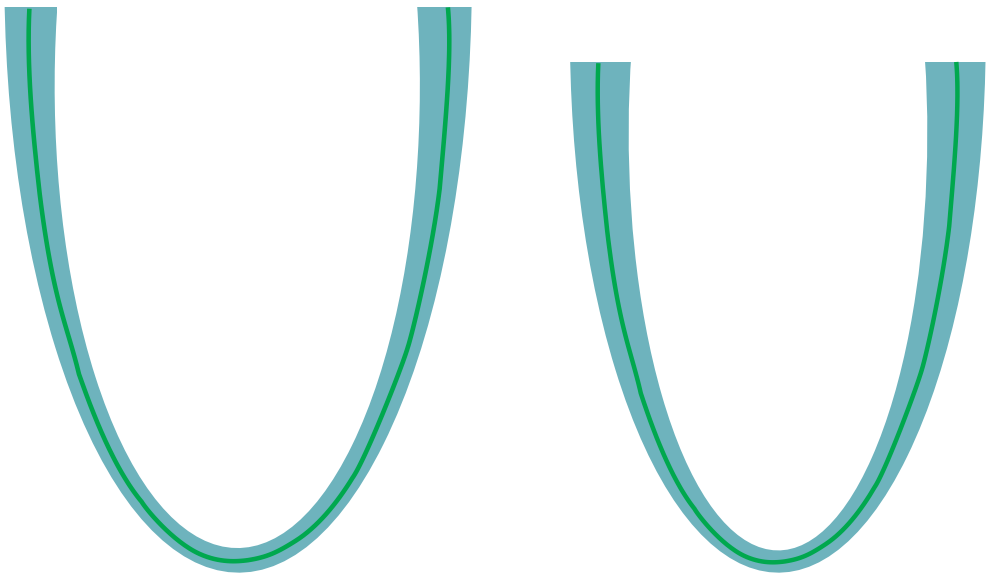

Figure 1.16: Schematic image depicting the measurement of longitudinal strain in the left ventricle. The left panel depicts the long axis in end diastole and right panel the long axis in end systole. Longitudinal strain is measured as the difference in length of the myocardium in the direction of the green line.

As the heart shortens in the longitudinal direction the circumference of the heart will also decrease. By measuring the length of the myocardium in the circumferential direction in end diastole compared to end systole we will get the relative circumferential shortening of the myocardium, or circumferential systolic strain [95] (Figure 1.17). The shortening in the longitudinal and circumferential direction leads to an increase in thickness of the myocardium. By measuring the thickness of the myocardium in end diastole compared to end systole we will get the relative thickening of the myocardium, or radial systolic strain [95] (Figure 1.17). The radial strain is only an effect of longitudinal and circumferential

shortening and is not a functional measure in itself.

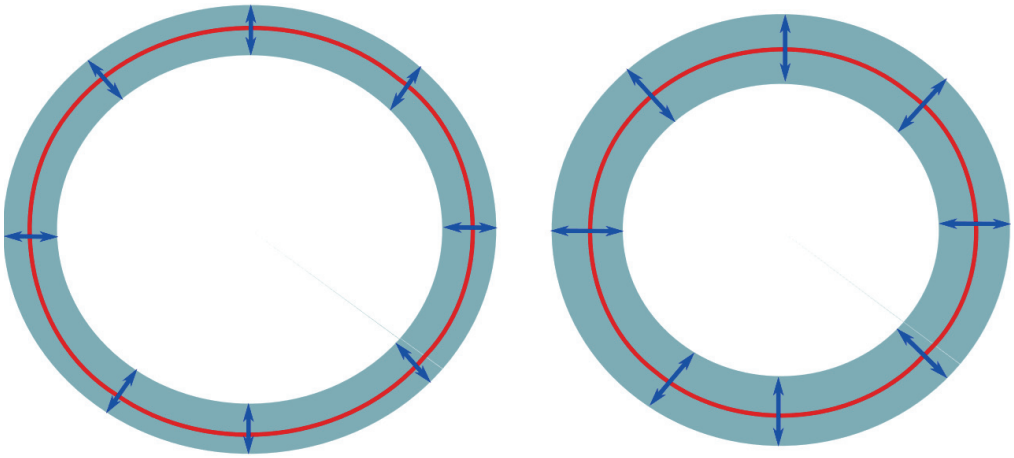

Figure 1.17: Schematic image depicting the measurement of circumferential and radial strain in the left ventricle. The left panel depicts the short axis in end diastole, right panel the short axis in end systole. Circumferential strain is measured as the difference in length of the myocardium in the direction of the red line and radial strain as the difference in length in the direction of the blue arrows.

The cardiac fibers are directed in a helical form through the LV with the fibers oriented more in a longitudinal direction in the endocardial and epicardial parts and more in a circumferential direction in the midmural part in the LV [96, 97]. In the RV there are only a few longitudinal fibers [98]. Strain is a description of the geometrical change in the myocardium and is not directly linked to fiber direction. There might be a correlation between fiber direction and strain direction, but it is hard to quantify to what degree. For example, although longitudinal function is the main contributor to stroke volume in the RV it doesn´t seem to be the case that longidutinal fibers are more abundant in the RV compared to the LV [98, 99]. There are no transmural fibers that could be responsible for radial function and radial strain is a function of shortening of longitudinal and circumferential fibers. Also, if there would be transmural fibers their contraction would result in thinning in the radial direction rather than thickening.

1.9 Atrioventricular plane displacement

When the ventricles contract the atrioventricular plane moves towards the apex of the heart. The movement of the atrioventricular plane from end diastole to end systole is called the atrioventricular plane displacement (AVPD) [99]. The AVPD is expressed in millimeters and is a measure of the cardiac pumping in the longitudinal direction, in this case meaning from the base to the apex. This means that the AVPD is measured in a different coordinate system compared to strain. Instead of defining the longitudinal direction as a line through

the myocardium, the longitudinal direction as the perpendicular direction from the atrioventricular plane from the base to the apex (Figure 1.18 and 3.9).

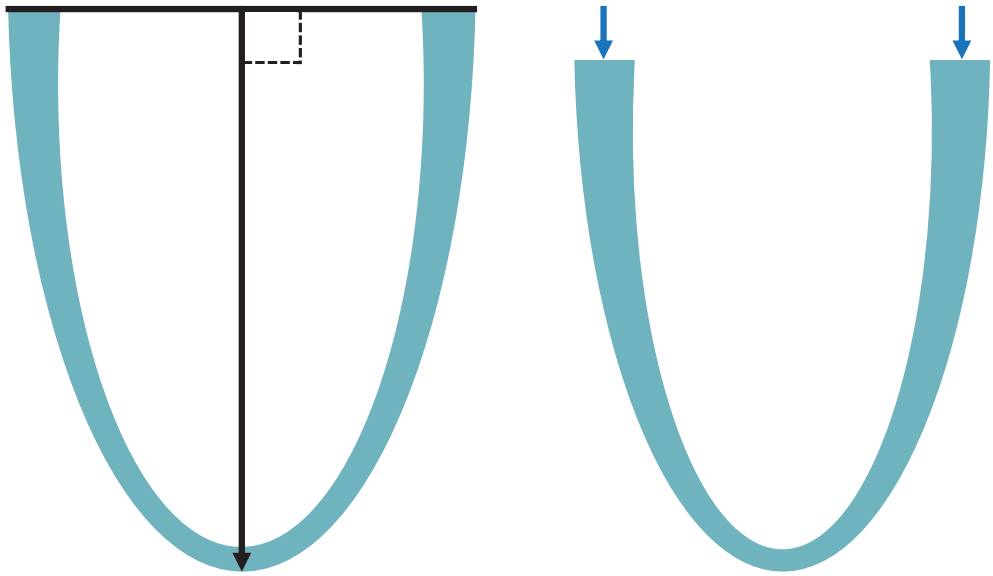

Figure 1.18: Atrioventricular plane displacement (AVPD) is measured perpendicular to the atrioventricular plane in the base to apex direction (black arrow). The distance that the atrioventricular plane moves from end diastole to end systole is the AVPD (blue arrows).

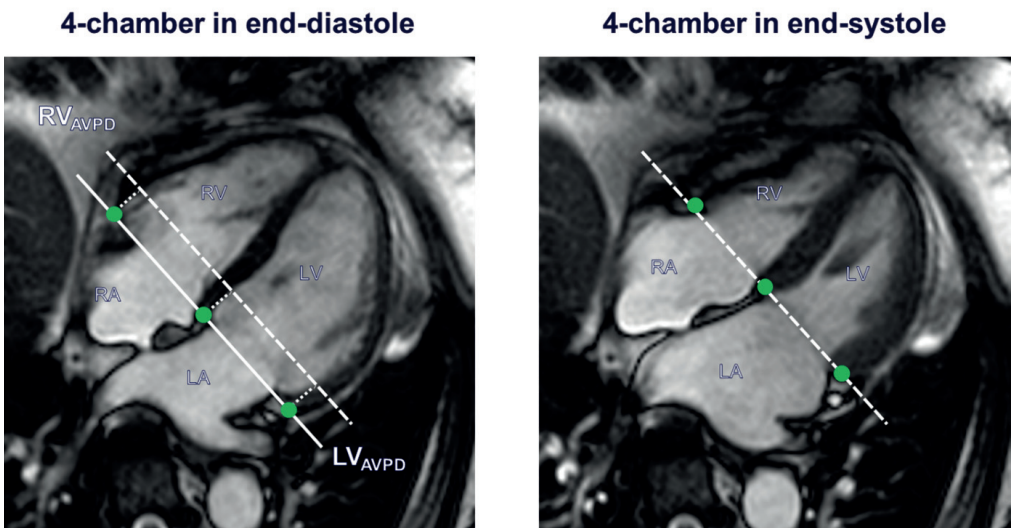

Figure 1.19: Representation of the atrioventricular displacement from end diastole to end systole. The atrioventricular plane in end diastole is represented as a solid line in the left panel and the atrioventricular plane in end systole is represented as a dashed line in the right panel. The end systolic line is here interpolated to the end-diastolic image. The atrioventricular plane displacement is the distance between the solid line in end diastole and the dashed line in end systole as shown to the left.

AVPD is a predictor of events in heart failure in the LV and is more sensitive than EF [100–102]. It has been shown that AVPD is lower in pulmonary hypertension compared to controls in both ventricles [103].

1.10 Regional contribution to stroke volume

Both strain and AVPD measures the regional contraction of the myocardium. However, it does not provide any information on how much the regional contraction contributes to stroke volume. When the atrioventricular plane moves towards the apex it works as a piston pump displacing a volume that can be calculated as AVPD multiplied by the area of the atrioventricular plane in the respective ventricle [99]. This volume is defined as the longitudinal stroke volume. The longitudinal stroke volume divided by total stroke volume gives a relative measure of how much of the total stroke volume is generated by longitudinal pumping. This is the longitudinal contribution to stroke volume.

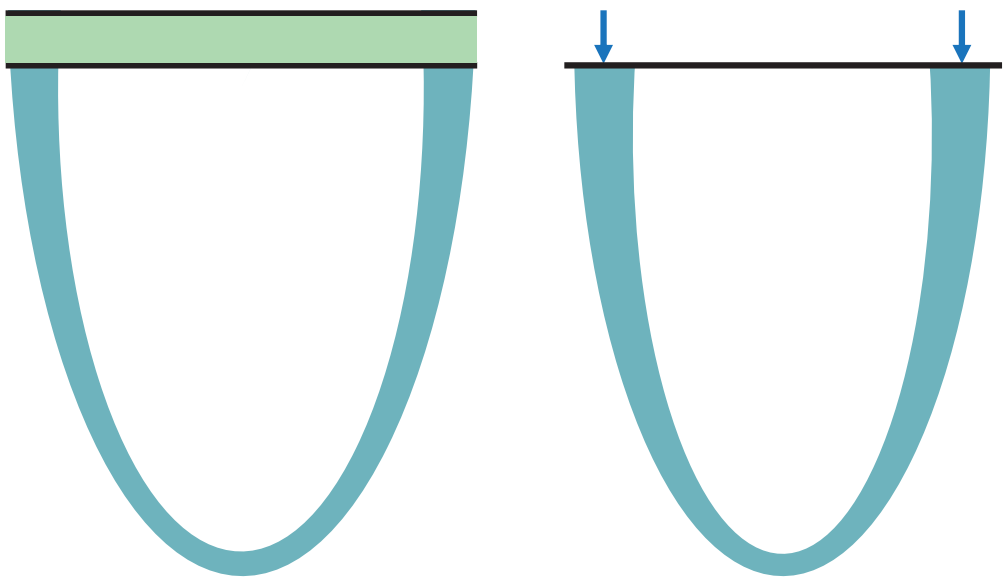

Figure 1.20: When the atrioventricular plane moves from the base towards the apex longitudinal stroke volume is calculated as the atrioventricular plane displacement (AVPD) multiplied by the area of the atrioventricular plane. The AVPD is noted with blue arrows and the longitudinal stroke volume is noted as the green area.

However, the heart does not only pump in a longitudinal motion but also by circumferential contraction. The effect of the circumferential contraction can be measured as the inward epicardial motion of the ventricular walls. The inward movement of the epicardial borders are defined as the radial stroke volume. This can in turn be divided into the lateral stroke volume, in the free wall and septal stroke volume, in the septum. The inward endocardial movement is an effect of both longitudinal and circumferential contraction.

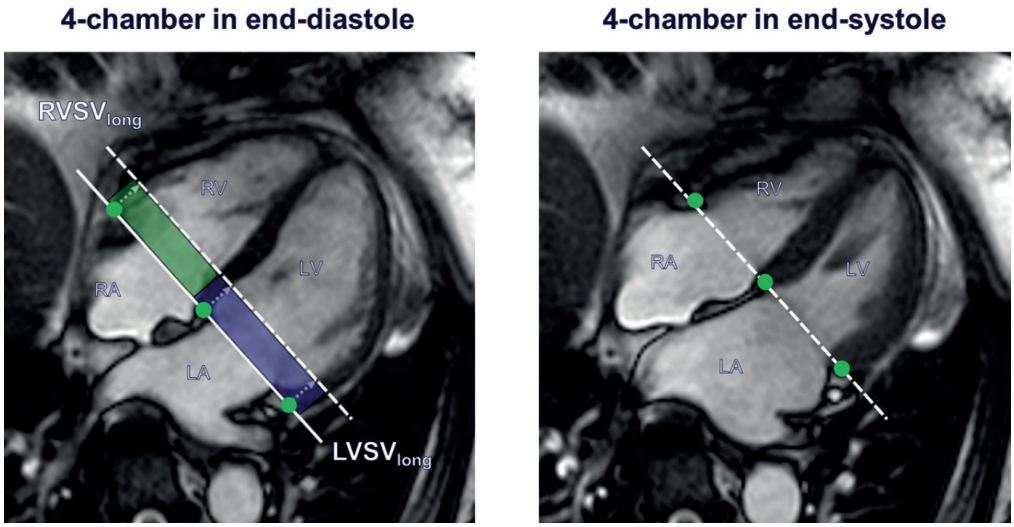

Figure 1.21: Visualization of longitudinal contribution to stroke volume in four-chamber view. The longitudinal contribution to stroke volume is computed as the volume encompassed by the atrioventricular plane displacement, here illustrated with blue color in the left ventricle and green color in the right ventricle.

Lateral stroke volume divided by total stroke volume is the lateral contribution to stroke volume. The septum is usually contributing to the stroke volume of the LV but with disease it can contribute to the RV stroke volume. The volume displaced by the septal movement either towards the LV or RV is defined as the septal stroke volume towards the ventricle it contracts towards. The septal contribution to stroke volume divided by stroke volume in each ventricle is the septal contribution to stroke volume. The septal contribution to stroke volume is therefore positive in one ventricle and negative in the other ventricle.

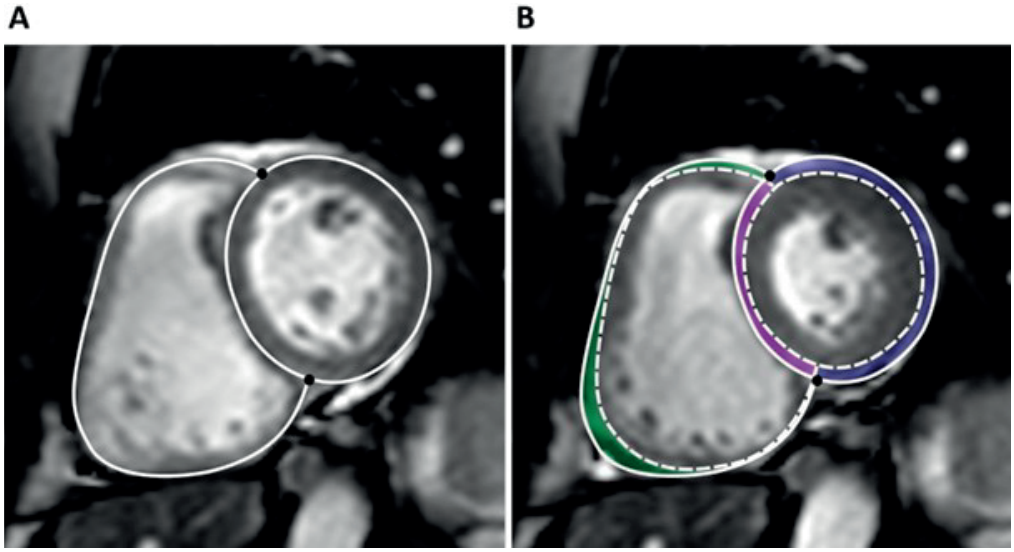

Figure 1.22: Cardiac magnetic resonance (CMR) images in short axis view. A Solid lines represent the epicardial borders and black circles RV insertions points at end diastole, and B dashed lines represent the epicardial borders at end systole. The end diastolic contour is interpolated to the end-systolic image. The area between the solid and dashed lines inside the RV insertion points (purple area, panel B) represents the septal contribution to stroke volume, which was summed from all short-axis slices. The area between the solid and dashed lines outside of the RV insertion points represent the lateral contribution to stroke volume, which was summed from all short-axis slices (green area, lateral contribution to RV, blue area lateral contribution to left ventricle). Adapted from The International Journal of Cardiovascular Imaging (2022) [104].

Chapter 2

2 Aims

The overall aim for this project was to evaluate novel CMR methods for diagnosis and risk assessment of PAH and to evaluate if these measures are related to invasive measurements.

Study I
To 1) evaluate whether LV and RV free wall global longitudinal strain differ between patients with systemic sclerosis, with and without PAH, compared to healthy controls, and 2) whether these differences are related to invasive measurements.

Study II
To 1) to investigate if LV longitudinal, radial and circumferential as well as RV longitudinal strain differ in cardiac asymptomatic systemic sclerosis patients with preserved EF compared to healthy controls, 2) to correlate the LV and RV deformation indices to clinical subsets and other disease characteristics and assess its potential clinical value.

Study III
To compare conventional and new RV function parameters derived from CMR to their echocardiographic equivalents in patients with pulmonary hypertension. Secondly, we aimed to investigate how these measures are associated with RVEF with CMR.

Study IV
To investigate if regional longitudinal and radial markers of biventricular function have prognostic implications in patients with PAH.

Study V
To determine if presence of post systolic contraction, duration of post systolic contraction and dyssynchrony are prognostic markers in PAH. A secondary aim was to investigate if a more comprehensive assessment from multiple CMR views improve the prognostication.

Chapter 3

3 Methods

3.1 Study population

All studies conform with the principles outlined in the Declaration of Helsinki. This means that participants had given written informed consent prior to study inclusion. All studies were approved by the Regional Ethical Review Board of Lund. There was an overlap between the study subjects in the studies in this thesis. The overlap in healthy controls is summarized in Table 3.1 and the overlap in patients in Table 3.2

Table 3.1: Overlap in healthy controls between the included subjects in this thesis.

	Study I	Study II	Study III	Study IV	Study V
Study I	-	19	0	2	0
Study II	19	-	0	0	0
Study III	0	0	-	0	0
Study IV	2	0	0	-	0
Study V	0	0	0	0	-

Table 3.2: Overlap in patients between the included subjects in this thesis.

	Study I	Study II	Study III	Study IV	Study V
Study I	-	38	11	17	16
Study II	38	-	5	0	0
Study III	11	5	-	20	23
Study IV	17	0	20	-	66
Study V	16	0	23	66	-

3.1.1 Study I

Sixty-five patients with systemic sclerosis were included at Skåne University Hospital (Lund, Sweden). Twenty-five of the patients had PAH. In addition to the patients, 19 healthy

volunteers from earlier studies in the group were analyzed [105–107]. Eight patients were excluded due to inadequate image quality or due to inadequate image protocol i.e., missing short axis stack, 2-,3- or 4-chamber view. After exclusion 57 patients and 19 volunteers were analyzed.

3.1.2 Study II

Fifty-four patients diagnosed with systemic sclerosis between were included. Thirty-eight of the patients that were previously analyzed in study I were included from Skåne University hospital (Lund, Sweden) with an additional 16 patients included from Onassis Cardiac Surgery Centre (Athens, Greece). Twenty-one controls were included, from Lund, for comparison

3.1.3 Study III

Ninety patients who had been evaluated for pulmonary hypertension at Skåne University Hospital (Lund, Sweden) were included. Twenty patients were excluded due to inadequate echocardiographic image quality, 15 patients due to atrial fibrillation, 12 when the endocardial borders were not traceable with echocardiography and 8 due to inadequate visualization of the RV with echocardiography. This left 55 patients for analysis.

3.1.4 Study IV

Seventy-six patients with PAH were included at Skåne University Hospital (Lund, Sweden). One patient was excluded due to inadequate image quality and four patients were excluded due to inadequate protocol i.e., missing 2-,3- or 4-chamber view. After exclusion, 71 subjects were analyzed. In addition CMR images from 20 healthy volunteers were included.

3.1.5 Study V

One-hundred-eighteen patients with PAH were included at Skåne University Hospital (Lund, Sweden). Two patients were excluded due to atrial septum defect, six due to atrial fibrillation, one due to aortic and mitral valve replacement, six due to insufficient image quality and two due to missing more than one of the required views. This left 101 patients for analysis.

3.2 Echocardiography

In study III Echocardiography was performed to make comparisons between echocardiography and CMR. The acquisition was performed with an iE33 ultrasound system (Philips Healthcare, Eindhoven, NL). Tricuspid annular plane systolic excursion, S'-wave velocity, myocardial strain derived from the RV lateral free wall and RV fractional area change were assessed from an apical 4-chamber RV focused view according to guidelines [108]. Acquisition was performed during end-expiratory breath-hold. Assessment was done using Xcelera (Philips Healthcare, Eindhoven, NL).

3.2.1 RV free wall strain

A dedicated software was used for strain analysis, CMQ, Q-lab 10.3 (Philips Healthcare, Eindhoven, NL). A region of interest was delineated in the RV endocardial border at end-diastole. Free wall strain by echocardiography was calculated as the average of the regional peak systolic strain from the three segments in the RV free wall (Figure 3.1).

3.2.2 Tricuspid annular plane systolic excursion

Tricuspid annular plane systolic excursion was measured by M-mode. The view was set up with the cursor optimally aligned along the direction of the tricuspid annulus and RV free wall. With the contraction of the RV the tricuspid annular movement can be plotted over time. The maximum distance of this movement is defined as the tricuspid annular plane systolic excursion (Figure 3.2).

3.2.3 S'-wave velocity

S'-wave velocity was measured with tissue doppler imaging with the tricuspid annulus aligned with the doppler cursor (Figure 3.3).

3.2.4 RV fractional area change

Fractional area change was defined as the fractional difference in area of the RV in the apical 4-chamber RV focused view between end-diastole and end-systole (Figure 3.4).

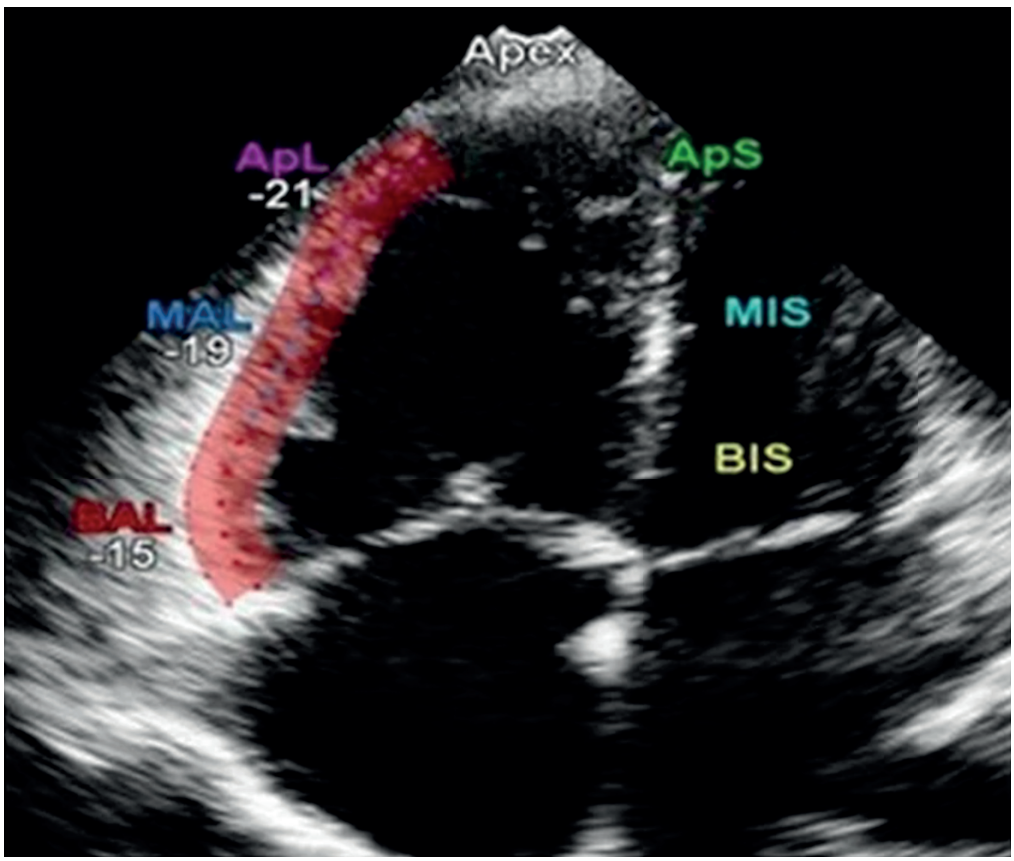

Figure 3.1: Illustration of echocardiographic assessment of RV free wall strain. Adapted from BMC Cardiovascular Disorders volume 20, Article number: 259 (2020) [109].

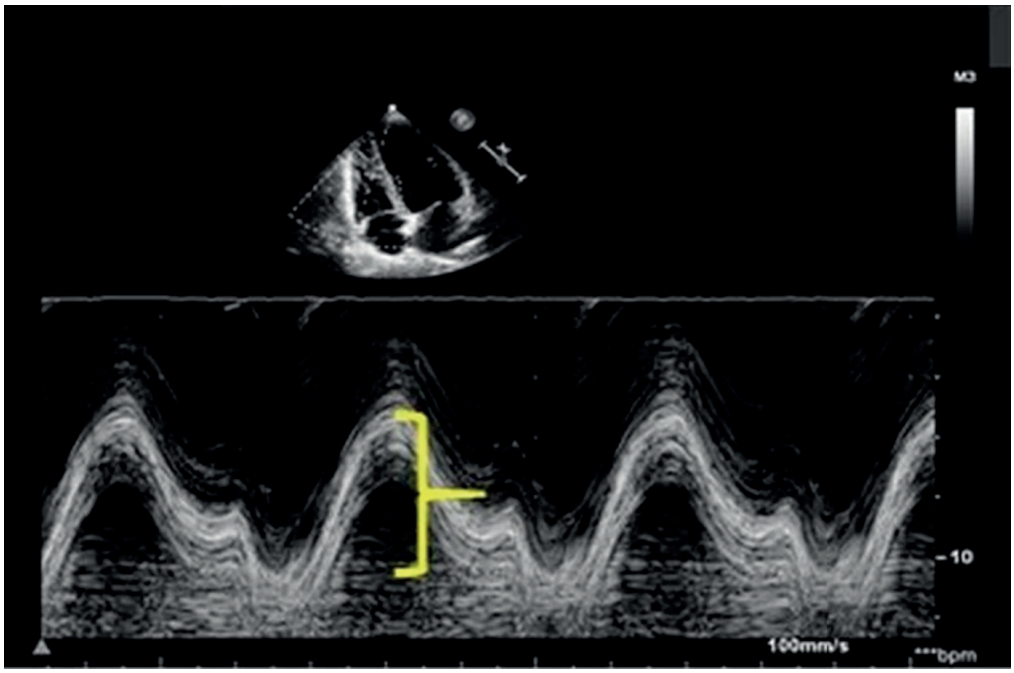

Figure 3.2: Illustration of echocardiographic assessment of tricuspid annular plane systolic excursion. Adapted from BMC Cardiovascular Disorders volume 20, Article number: 259 (2020) [109].

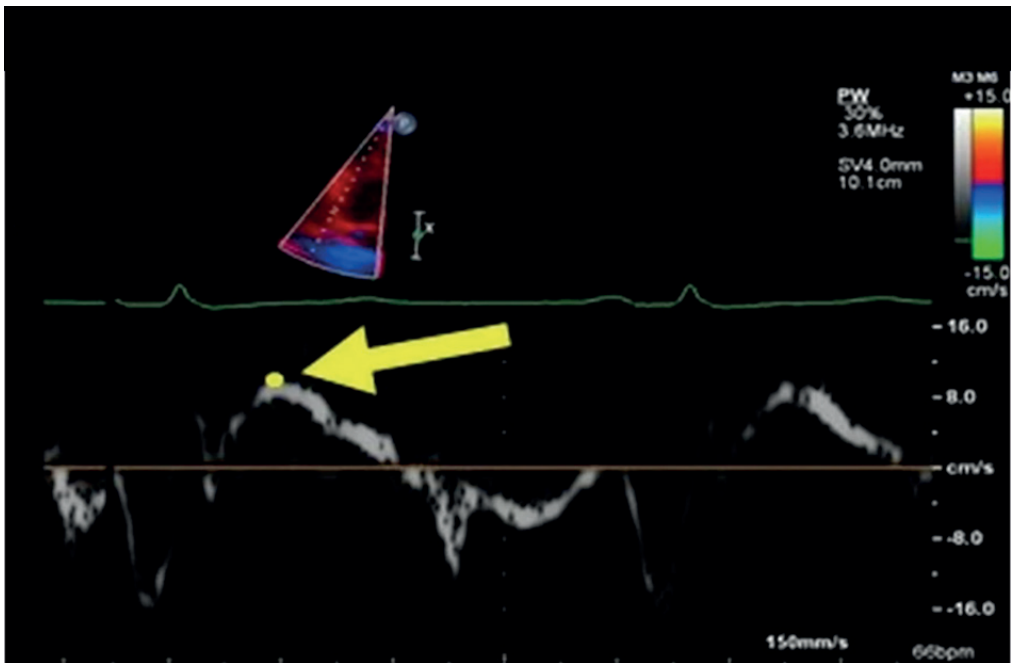

Figure 3.3: Illustration of echocardiographic assessment of S' wave velocity. Adapted from BMC Cardiovascular Disorders volume 20, Article number: 259 (2020) [109].

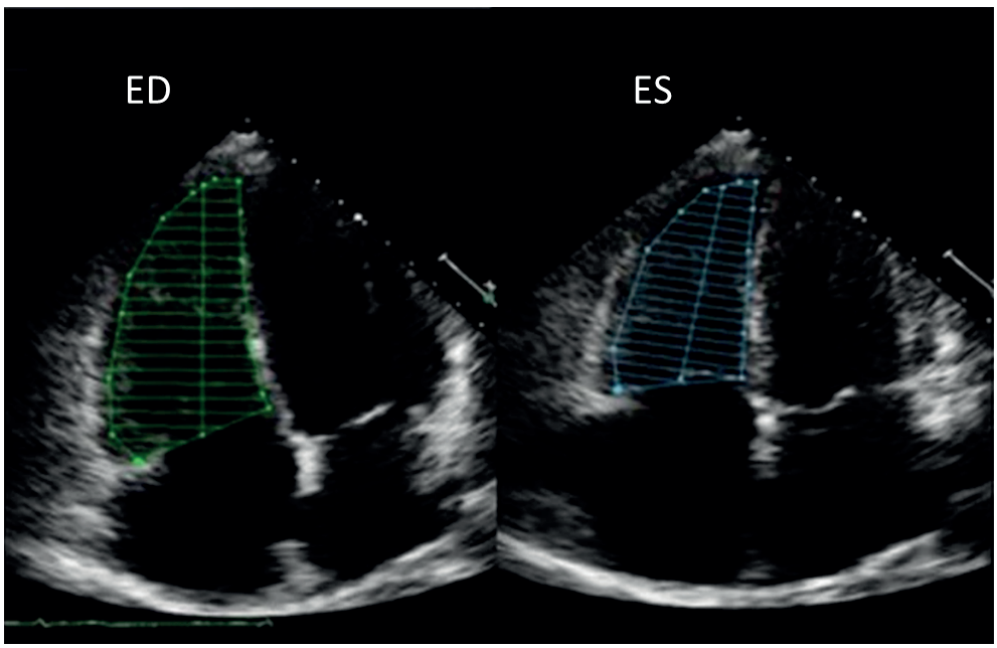

Figure 3.4: Illustration of echocardiographic assessment of RV fraction area change. The fractional area change was calculated as the fractional difference in area in end diastole (ED) and end systole (ES). Adapted from BMC Cardiovascular Disorders volume 20, Article number: 259 (2020) [109].

3.3 Cardiac magnetic resonance imaging

CMR was used in all studies (study I-V). The main novel methods in this thesis have been myocardial strain, AVPD and regional contribution to stroke volume. In addition assessment of post systolic strain was made from myocardial strain. All of the studies have used standard cine images for the analysis.

3.3.1 Image acquisition

Two scanners were used for CMR examination for the studies in this thesis. Until 2015 scans were performed with a 1.5 Tesla Philips Achieva system *(Philips Healthcare, Best, The Netherlands)*. From 2015 a 1.5 T Siemens Aera was used for scans *(MAGETOM Aera, Siemens Healthcare, Erlangen, Germany)*. Scans were performed with the subjects in supine position during end-expiratory breath-hold with a cardiac coil and ECG-triggering. Standard cine balanced steady state free precession images were used for all studies. For Philips, typical image parameters were: 60° flip angle, temporal resolution of 47 ms reconstructed to 30 time phases per cardiac cycle, repetition time of 3 ms, 1.4 ms echo time, 8 mm slice thickness with no slice gap and in-plane resolution of 1.5x1.5 mm. For Siemens typical parameters were: 60° flip angle, temporal resolution of 46 ms reconstructed to 25 time phases per cardiac, repetition time of 3 ms, 1.4 ms echo time, 6 mm slice thickness with 2 mm slice gap and in-plane resolution of 0.8x0.8 mm. For this thesis short axis stack, 2-chamber, 3-chamber, 4-chamber, RV 3-chamber and right ventricular outflow tract-views were used (Figure 3.5). The specific views for the studies are presented in table 3.3.

Table 3.3: Views used in the included manuscripts for this thesis.

Study/view	SAX	2-ch	3-ch	4-ch	RV3-ch	RVOT
I	x	x	x	x		
II	x			x		
III	x			x		
IV	x	x	x	x		
V	x	x	x	x	x	x

SAX, short axis stack;2-ch, 2-chamber view; 3-ch, 3-chamber view; 4-ch, 4-chamber view; RV3-ch, RV3-chamber view; RVOT, right ventricular outflow tract.

In study II and IV late gadolinium images were analyzed. Gadolinium-based contrast agent was given as part of standard protocol to the patients with PAH if kidney function allowed. Late gadolinium images were acquired 15–20 min after injection of gadolinium contrast. According to clinical protocol, late gadolinium images were acquired in the long axis views collected in cine as well as a basal, midventricular and apical slice in the short axis stack.

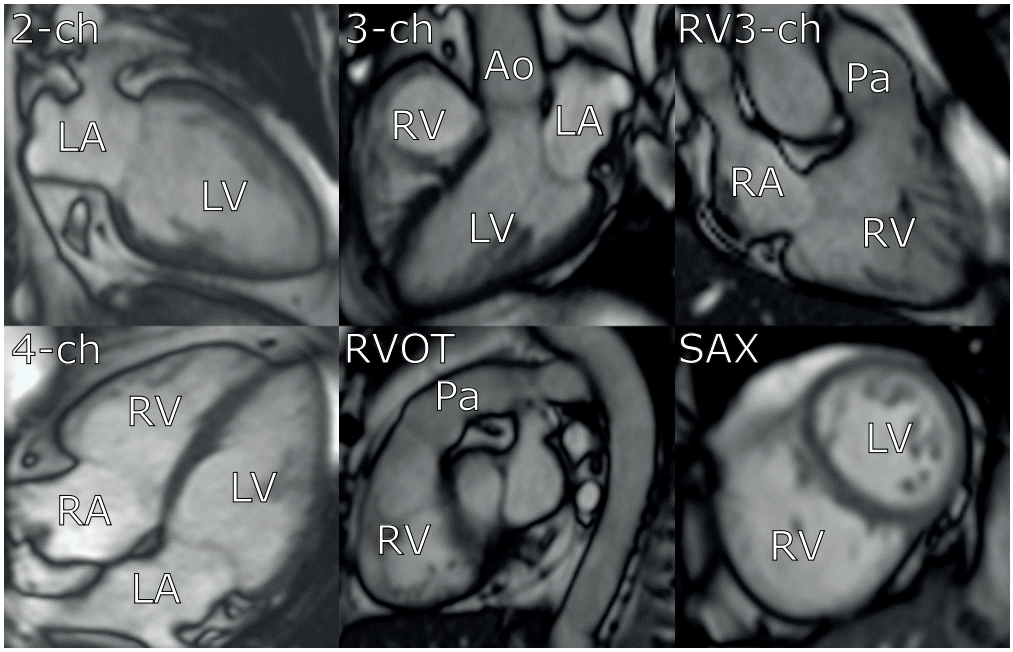

Figure 3.5: Example of the views used in this thesis from a PAH patient. 2-ch, 2-chamber view; 3-ch, 3-chamber view; RV3-ch, right ventricular 3-chamber view; 4-ch, 4-chamber view; RVOT, right ventricular outflow tract; SAX, short axis stack; LV, left ventricle; LA, left atrium; Ao, aorta; RV, right ventricle; RA, right atrium; Pa, pulmonary artery.

3.3.2 Image analysis

Image analysis for CMR was performed with two different software's. For study I and II image analysis were performed with Circle CVI 42 (Circle Cardiovascular Imaging Inc. Calgary, AB, Canada) and for study III, IV and V image analysis was performed with the freely available software Segment (http://segment.heiberg.se) [110].

3.3.3 Cardiac volumes and function

Cardiac volumes and function were calculated from manual delineations of the endocardial borders in the short axis stack in both ventricles. The end-diastolic and end-systolic volumes were calculated from the volume encompassed by the endocardial border in all short axis slices with visual ventricular mass in end diastole and end systole (Figure 3.6).
Stroke volume was calculated as the difference between the end diastolic volume and the end systolic volume. EF was calculated as stroke volume divided by the end diastolic volume.

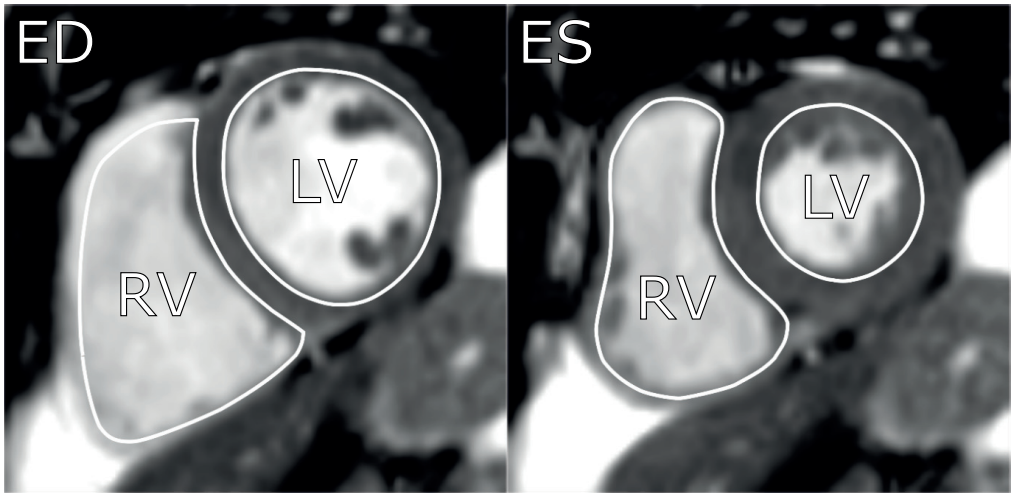

Figure 3.6: Example of the delineations from a slice from short axis stack with end diastole (ED) in the left panel and end systole (ES) in the right panel. Volumes were caclulated as the volumes encompassed by the endocardial borders when all short axis slices were added. LV,left ventricle; RV, right ventricle.

3.3.4 Strain

Strain was analyzed by manually delineating the myocardial borders in end diastole whereafter an automated tracking was performed by software through the cardiac cycle (Figure 3.7). For the cases where tracking was not adequate the delineations were modified, and new tracking was performed. This was reiterated until the tracking was adequate.

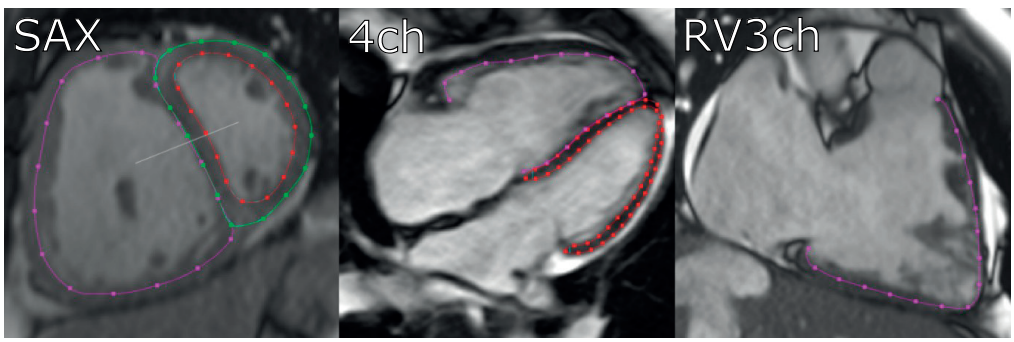

Figure 3.7: Examples of strain delineations in end diastole from a short axis slice (SAX), 4-chamber view (4ch) and right ventricular 3-chamber view RV3ch. The red line in SAX represents the endocardial border and the green line the epicardial border in the left ventricle. The red line in 4ch represents the endocardial and epicardial borders in the left ventricle. The purple line represents delineation of the endocardial border of the right ventricle.

3.3.5 Tricuspid annular plane systolic excursion and S'

Tricuspid annular plane systolic excursion from CMR was analyzed in study III (AVPDlat) and study IV (CMR-TAPSE) (Figure 3.8). This was calculated by measuring the displacement of the most basal point in the lateral RV wall between end diastole and end systole. S' was derived from the derivative of the time resolved tricuspid annular plane systolic excursion curve.

3.3.6 RV fractional area change

Fractional area change was calculated as the difference in area encompassed by the endocardial borders from the 4-chamber view between end diastole and end systole. (Figure 3.8).

3.3.7 Atrioventricular plane displacement

Eight points were manually placed in end diastole and end systole in the base of the ventricular myocardium in 2-chamber, 3-chamber and 4 chamber view (Figure 3.9). AVPD defined as the mean longitudinal displacement, perpendicular to the atrioventricular plane, from end diastole to end systole in six points in the LV and in four points in the RV (Figure 3.9).

3.3.8 Regional contribution to stroke volume

Longitudinal contribution to stroke volume was calculated with a validated method, as AVPD multiplied with mean short-axis epicardial area from the two largest LV slices or the three largest RV slices divided by stroke volume (Figure 3.10) [99]. The lateral contribution to stroke volume was computed as the difference between the epicardial volumes in ED and ES, with the septal volume subtracted, divided by stroke volume [99]. The septal contribution to stroke volume was computed as the volume displaced by the movement of the septum divided by stroke volume (Figure 3.11).

3.4 Right heart catheterization

For study I, III, IV and V patients underwent right heart catheterization. This was performed using a triple lumen Swan-Ganz catheter under local anesthesia in supine position. Pressures in the right atrium, right ventricle, the pulmonary artery as well as pulmonary

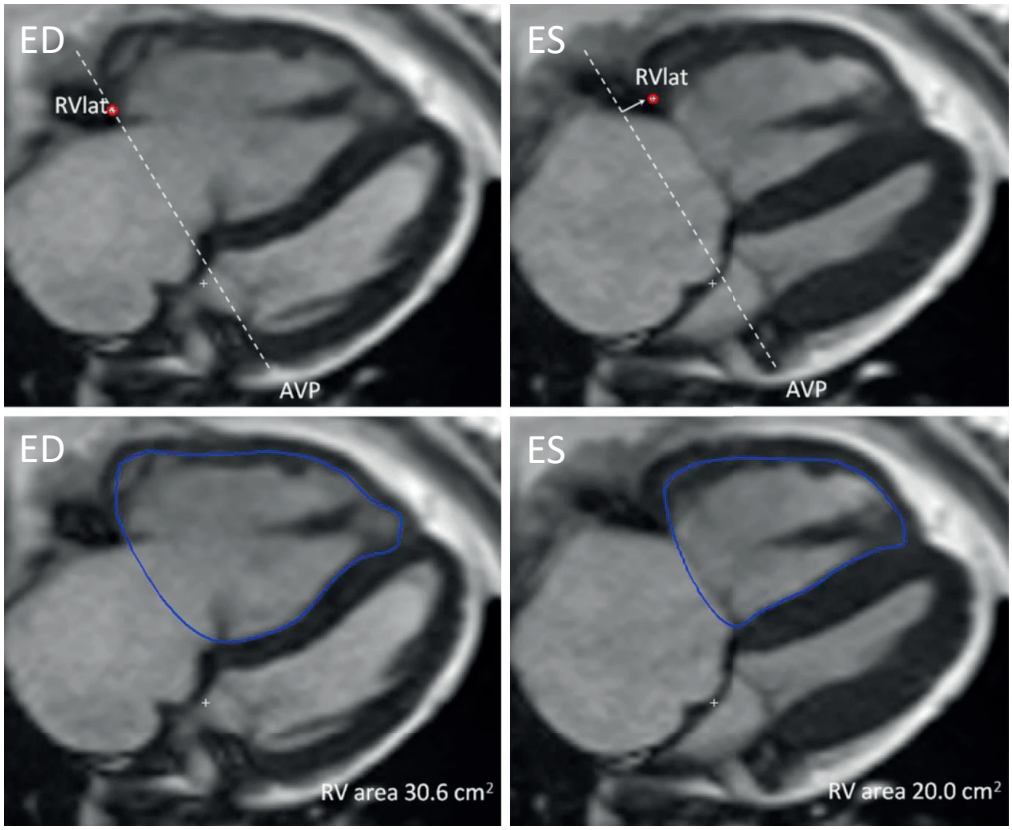

Figure 3.8: Examples of lateral atrioventricular plane displacement, upper panels, and fractional area change, lower panels, in the right ventricle (RV). End diastole (ED) in the left panels and end systole (ES) in the right panels. Lateral atrioventricular plane displacement was calculated as the distance between the basal part of the RV free wall (RVlat) from ED to ES, perpendicular to the atrioventricular plane in ED. Fractional area change was calculated as the difference in RV area from ED to ES, delineated in blue. Adapted from BMC Cardiovascular Disorders volume 20, Article number: 259 (2020) [109].

artery wedge pressure was measured during free breathing over several heart beats. Cardiac output was derived from thermodilution. In addition, mixed venous saturation was measured.

3.5 Statistical analysis

The statistical software's used for the studies in this thesis were IBM SPSS Statistics 23,25 and 28 (Armonk, NY, USA, IBM Corp) and GraphPad Prism 7 (La Jolla, CA, USA, GraphPad Software, Inc). Continuous variables were expressed as mean ± standard deviation and 95% confidence interval, or median and interquartile range according to normal distribution, with normal distribution assessed visually with histograms or with Shapiro–Wilk tests.

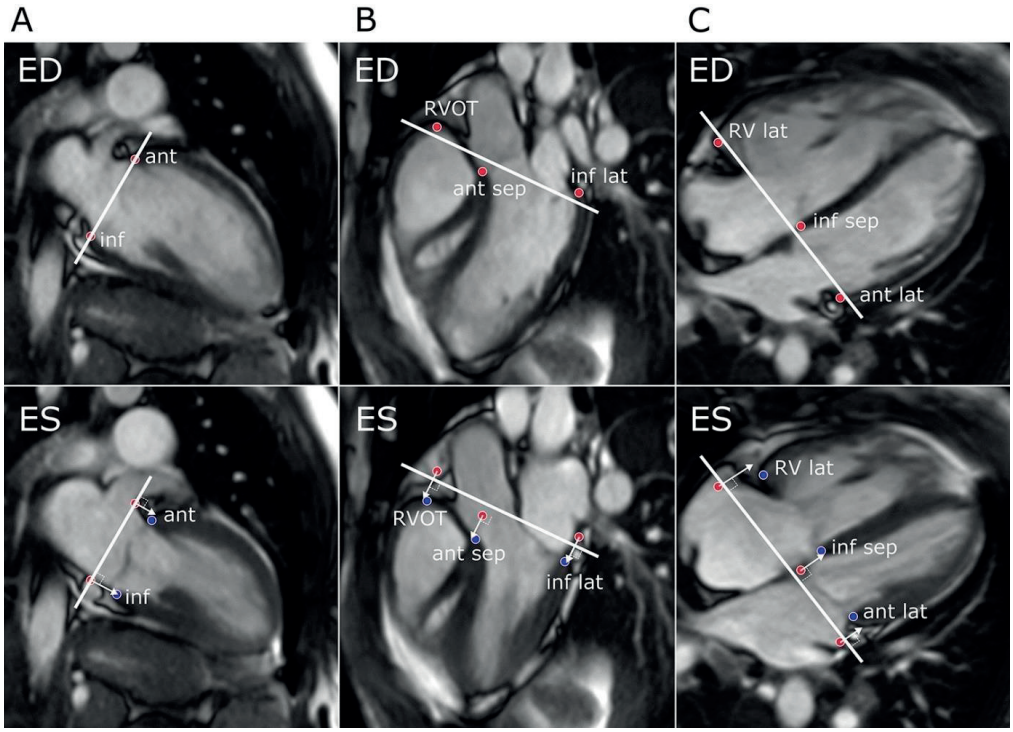

Figure 3.9: Example of atrioventricular plane displacement with end diastole (ED) in the upper row and end systole in the lower row (ES). A. Two points were placed in the anterior (ant) and inferior (inf) points in the 2-chamber view. B. Three points were placed in the inferior lateral (inf lat) wall, the anterior septal wall (ant sep) and the right ventricular outflow tract (RVOT). C. Three points were place in the right ventricular lateral wall (RV lat), inferior septal wall (inf sep) and in the anterior lateral wall (ant lat). The atrioventricular plane was defined in end diastole. The atrioventricular plane displacement was calculated as the mean of the displacement of the six points in the left ventricle and the four points in the right ventricle. Adapted from Int J Cardiovasc Imaging (2022). [104].

Categorical variables were expressed as absolute numbers and proportion. Group comparisons were performed with one-way ANOVA and independent samples t-test for parametric data. For comparison between multiple groups, one-way ANOVA in conjunction with Tukey post hoc analysis was used. Kruskal–Wallis and Mann-Whitney U-test was used for non-parametric data. Chi-square was used for nominal data. Linear regression with Pearson's correlation was used for correlation analyses. For cut-off value calculation with receiver operating characteristic, a sum of squares method was used [111]. Kaplan–Meier plots were used for survival curves with Cox regression analysis for calculating hazard ratio and log-rank test for p-values. Cox regression analysis was performed as univariate and bivariate analysis for continuous variables. Statistical significance was assumed when a two-sided P-value was <0·05.

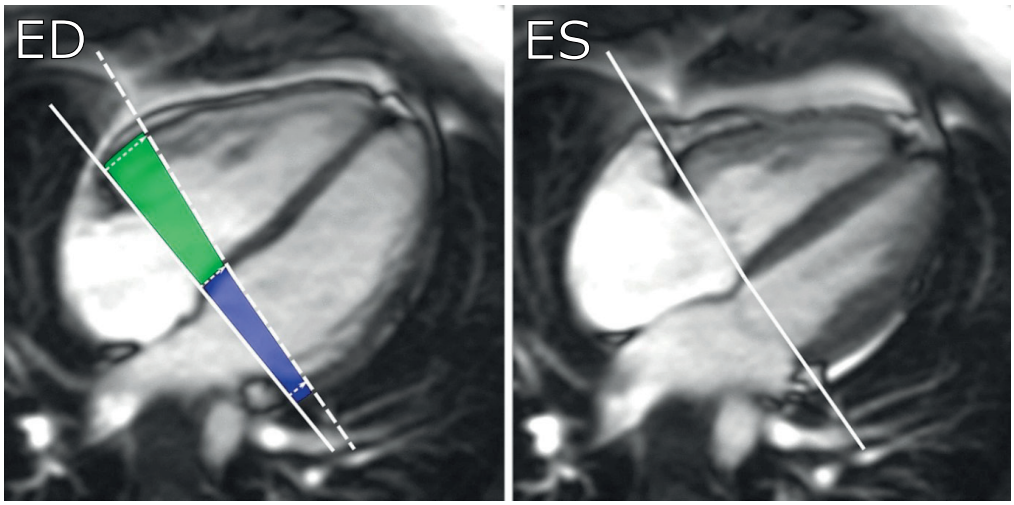

Figure 3.10: Example of longitudinal contribution to stroke volume. The solid lines represent the atrioventricular plane in end diastole (ED) and end systole (ES). The dashed line represents the atrioventricular plane in ES interpolated to the ED image. The longitudinal contribution to stroke volume is here visualized as the volume encompassed by the blue area in the left ventricle and by the green area in the right ventricle. Adapted from Int J Cardiovasc Imaging (2022). [104].

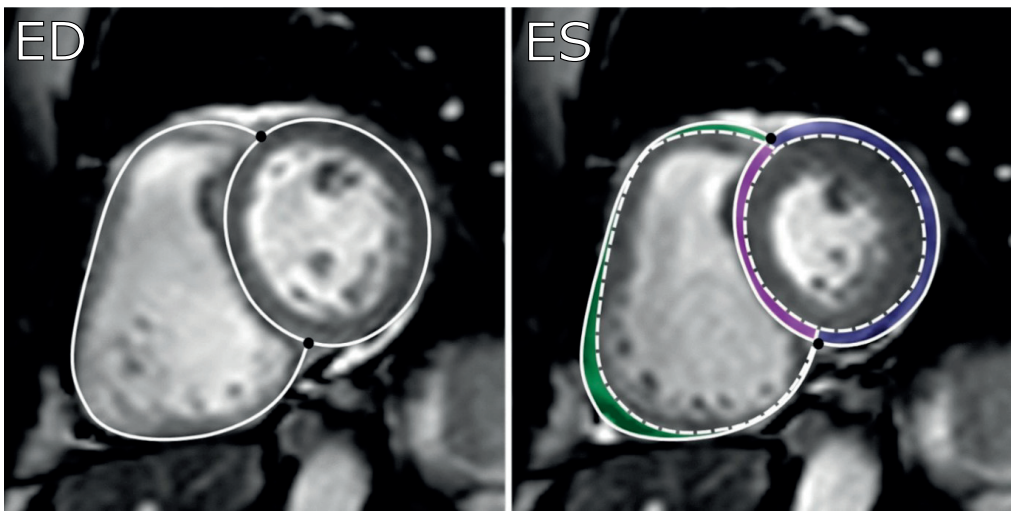

Figure 3.11: Example of lateral and septal contribution to stroke volume. The solid lines represent the epicardial borders in end diastole (ED) and the dashed line in end systole (ES). The area that are displaced between ED and ES, when added for all slices, were defined as the lateral contribution to stroke volume in the left ventricle in blue and for the right ventricle in green when divided by stroke volume. The septal contribution to stroke volume was defined as the volume displaced by the purple area when divided by stroke volume. Adapted from Int J Cardiovasc Imaging (2022). [104].

Chapter 4

4 Results

4.1 Study I

Peak global longitudinal strain (GLS) was lower in PAH patients with systemic sclerosis in both ventricles compared to both patients with systemic sclerosis without PAH and controls (LV: P = 0·01, RV: P<0·001) (Table 4.1). There was no difference in GLS in either ventricle between patients with systemic sclerosis without PAH and controls (Figure 4.1). Strain values are presented in table 4.1. GLS in the LV and RV free wall correlated with mPAP and pulmonary vascular resistance (Figure 4.3).

Table 4.1: Strain values for patients with systemic sclerosis with pulmonary arterial hypertension (PH), systemic sclerosis without PAH and controls.

	Systemic sclerosis with PH	Systemic sclerosis without PH	Controls
Left ventricle	–18 ± 3%	–20 ± 3%	–20 ± 2%
Right ventricle	–20 ± 6%	–28 ± 4%	–28 ± 2%

Receiver operating characteristics for RV free wall GLS predicting the diagnosis of PAH in patients with systemic sclerosis had an area under the curve of 0.86 with LV GLS having an area under the curve of 0.73. With a cut-off value of RV free wall GLS at –26.2% sensitivity was 84% and specificity was 77% for the diagnosis of PAH. With a cut-off value of LV GLS at –20·0% sensitivity was 84% and specificity was 58% (Figure 4.2).

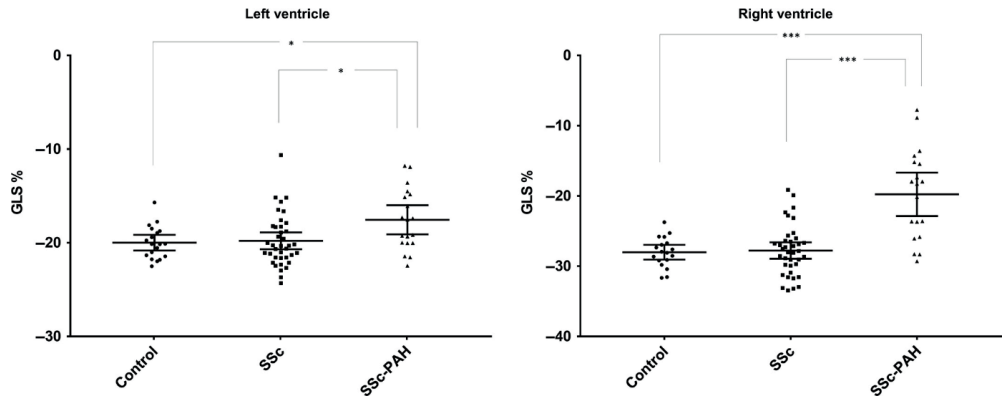

Figure 4.1: Peak global longitudinal strain (GLS) presented as mean ± 95 confidence interval in the left ventricle to the left and the right ventricle to the right. Control, healthy controls; SSc, systemic sclerosis; SSc-PAH, systemic sclerosis and pulmonary arterial hypertension

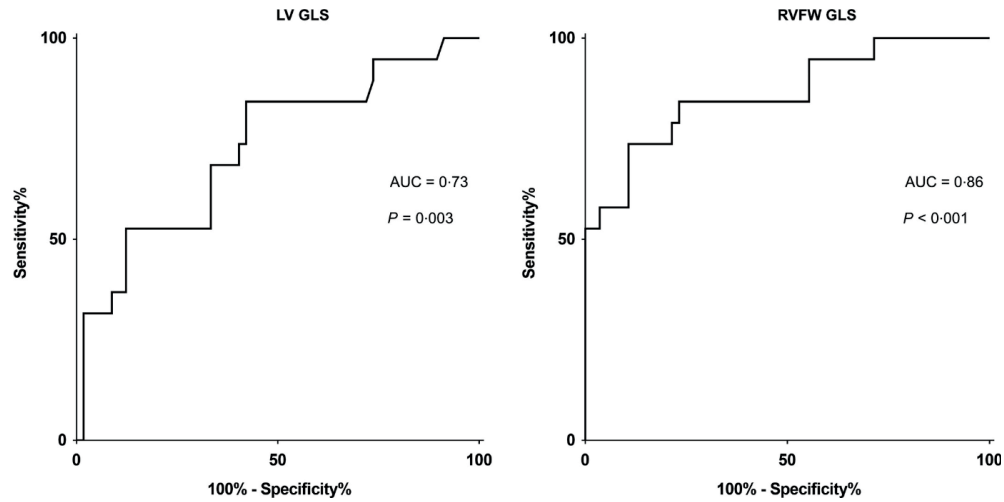

Figure 4.2: Receiver operating characteristics analyses for peak global longitudinal left ventricular strain (LV GLS) and right ventricular free wall (RVFW GLS). AUC, area under the curve.

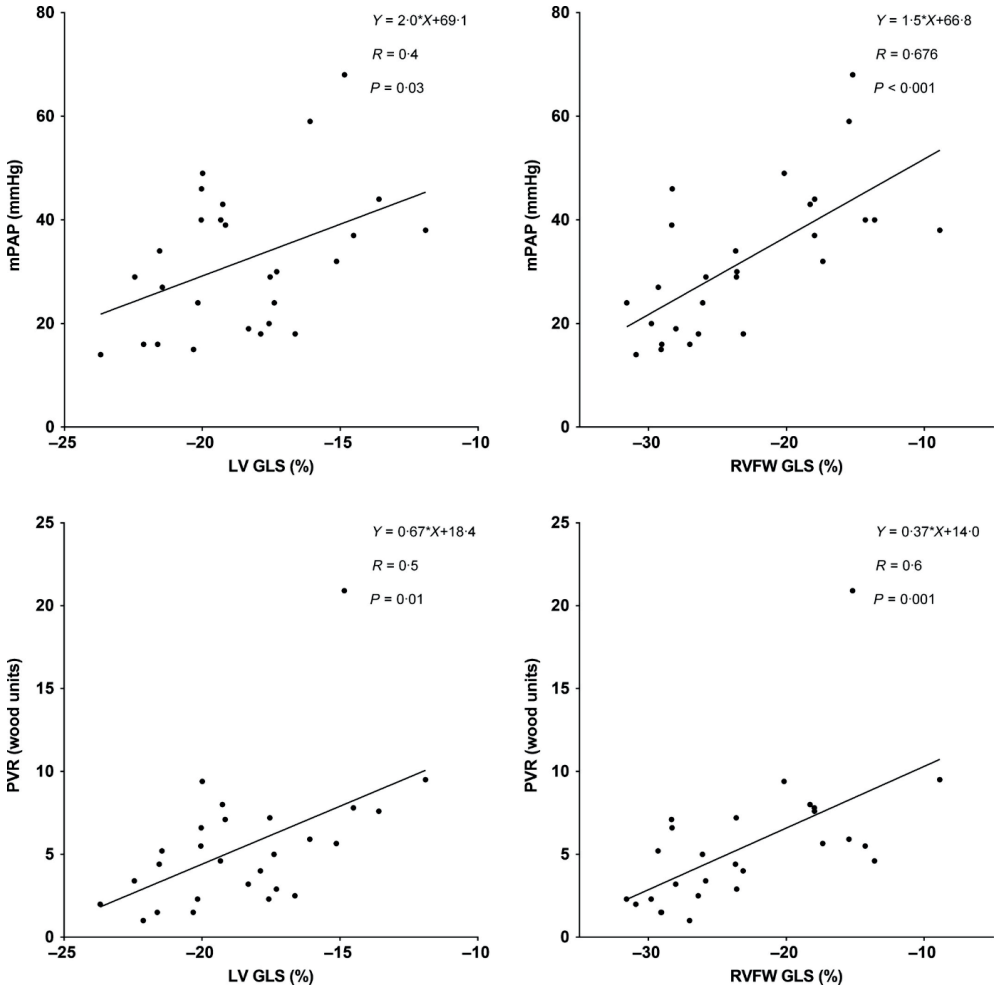

Figure 4.3: Correlation between peak global longitudinal left ventricular strain (LV GLS) in the left panel and right ventricular free wall (RVFW GLS) in the right panel. Comparisons with mean pulmonary arterial pressure (mPAP) in the top panel and pulmonary vascular resistance (PVR) in the bottom panel.

4.2 Study II

Patients with systemic sclerosis had lower RV free wall GLS and strain rate compared to controls ($p < 0.001$ and $p = 0.01$, respectively) (Table 4.2). Patients with digital ulcers had significantly lower circumferential strain compared to patients without digital ulcers (Table 4.2). LV GLS was lower in patients with insertion fibrosis and in patients with infarction compared to patients without fibrosis (Table 4.2).

Table 4.2: Cardiac magnetic resonance (CMR) functional, volumetric and strain data controls, patients with systemic sclerosis (SSc) and subgroups of SSc.

	Controls (n = 21)	SSc (n = 54)	P-value[A]	Diffuse SSc (n = 24)	Limited SSc (n = 30)	P-value[B]	No Digital Ulcer (n = 41)	Digital Ulcer (n = 13)	P-value[C]
Left ventricle									
LVEF (%)	59±5	62±6	0.01	63±5	62±7	0.4	61±6	65±3	0.02
LVEDV (ml)	156±26	131±28	0.001	131±25	131±30	0.8	132±28	129±26	0.7
LVESV (ml)	65±14	50±15	< 0.001	49±12	51±16	0.7	51±15	46±11	0.2
LVSV (ml)	89±17	79±17	0.04	84±13	78±18	0.3	79±17	83±17	0.5
Strain (Mid radial)	44.5±8.5 (n = 19)[D]	42.2±11.8 (n = 52)[E]	0.4	38.7±12.2 (n = 22)	44.8±11.0	0.07	43.4±12	37.9±11 (n = 11)	0.2
Strain rate (Mid radial)	2.4±0.72 (n = 19)	2.5±0.82 (n = 47)[F]	0.7	2.3±0.75 (n = 17)	2.6±0.85	0.2	2.5±0.80 (n = 38)	2.3±0.91 (n = 9)	0.3
Strain (Mid circumferential)	-21.9±2.8 (n = 19)	-21.6±3.2 (n = 52)[E]	0.7	-20.9±3.7 (n = 22)	-22.1±3.0	0.2	22.1±3.0	-19.7±3.4 (n = 11)	0.02
Strain rate (Mid circumferential)	-1.0±0.57 (n = 19)	-1.3±0.37 (n = 47)[F]	0.07	-1.2±0.42 (n = 17)	-1.3±0.34	0.6	1.3±0.37 (n = 38)	-1.1±0.34 (n = 9)	0.1
Strain (Longitudinal)	-20.3±2.5	-19.4±3.2	0.3	-18.9±2.9	-19.8±3.4	0.3	19.7±3.1	-18.8±3.4	0.4
Strain rate (Longitudinal)	-1.1±0.21	-1.2±0.35 (n = 49)[G]	0.5	-1.1±0.36 (n = 19)	1.1±0.28	0.6	1.1±0.32 (n = 38)	-1.1±0.29 (n = 11)	0.5
Right ventricle									
RVEF (%)	58±6	59±9	0.8	56±10	60±7	0.08	59±7	57±12	0.4
RVEDV (ml)	164±34	129±37	< 0.001	131±49	127±25	0.7	133±39	115±31	0.1
RVESV (ml)	68±19	54±26	0.04	59±35	51±16	0.3	56±26	50±25	0.5
RVSV (ml)	94±23	74±17	< 0.001	72±20	76±15	0.4	77±16	65±18	0.03
Strain (Longitudinal)	-28.2±2.0 (n = 20)[H]	-27.0±4.0	0.01	-25.9±4.4	-27.9±3.4	0.07	27.4±3.9	-26.0±4.2	0.3

Strain is measured in (%), Strain rate is measured in (1/s) expressed in mean±SD.

[A]: controls versus all SSc,

[B]: diffuse versus limited cutaneous SSc,

[C]: without versus with digital ulcers.

[D]: Two controls had inadequate image acquisition for radial and circumferential tracking,

[E]: Two patients had artefacts,

[F]: 7 had no time data for strain rate analysis in short axis images,

[G]: Five patients had not time data for strain rate analysis in 4-chamber view,

[H]: One control had inadequate tracking for RV strain analysis.

Control = Healthy adult volunteers; SSc = Systemic sclerosis; LVEF = Left ventricular ejection fraction; LVEDV = Left ventricular end diastolic volume; LVESV = Left ventricular end systolic volume; LVSV = Left ventricular stroke volume; RVEF = Right ventricular ejection fraction; RVEDV = Right ventricular end diastolic volume; RVESV = Right ventricular end systolic volume; RVSV = Right ventricular stroke volume

https://doi.org/10.1371/journal.pone.0221021.t002

4.3 Study III

There were significant correlations between RV fractional area change with CMR and echocardiography, lateral AVPD with CMR and tricuspid annular systolic excursion with echocardiography, max emptying velocity (S') with CMR and echocardiography and RV free

wall GLS with CMR and echocardiography (Figure 4.4). The absolute and relative bias and between CMR and echocardiography was 5.1 ± 8.4%/18.5 ± 32.5% for fractional area change, 5.5 ± 4.6 mm/33.2 ± 25.2% for lateral AVPD and tricuspid annular systolic excursion, 2.4 ± 3.0 cm/s/24.1 ± 28.3% for S' and 4.4 ± 5.8%/20.2 ± 37.5% for RV free wall GLS (Figure 4.4).

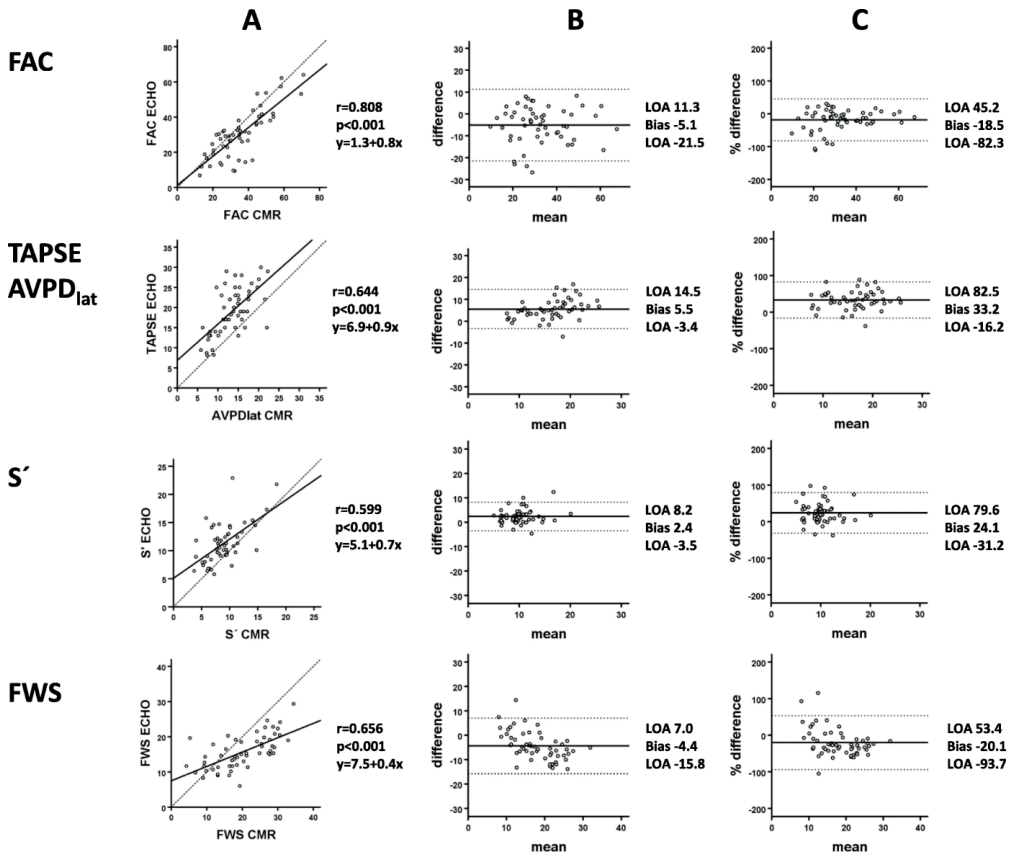

Figure 4.4: Panel A, correlation between cardiac magnetic resonance (CMR) derived parameters compared to corresponding echocardiographic (ECHO) derived parameters. Panel B, Bland-Altman plots showing the agreement of the parameters between CMR and ECHO in absolute numbers. C, Bland-Altman plots showing the relative agreements of the parameters between CMR and ECHO in percentages. FAC, fractional area change; TAPSE, tricuspid annular systolic excursion; AVPDlat, lateral atrioventricular plane displacement; S', max emptying velocity; FWS, free wall strain, free wall strain; LOA, level of agreement.

Fractional area change with CMR and RV free wall strain with echocardiography showed strong correlation when compared with EF in the RV, measured with CMR. Fractional area change and tricuspid annular systolic excursion with echocardiography, lateral AVPD and RV free wall GLS with CMR showed moderate correlation. S' showed weak correlation with both CMR and echocardiography (4.5).

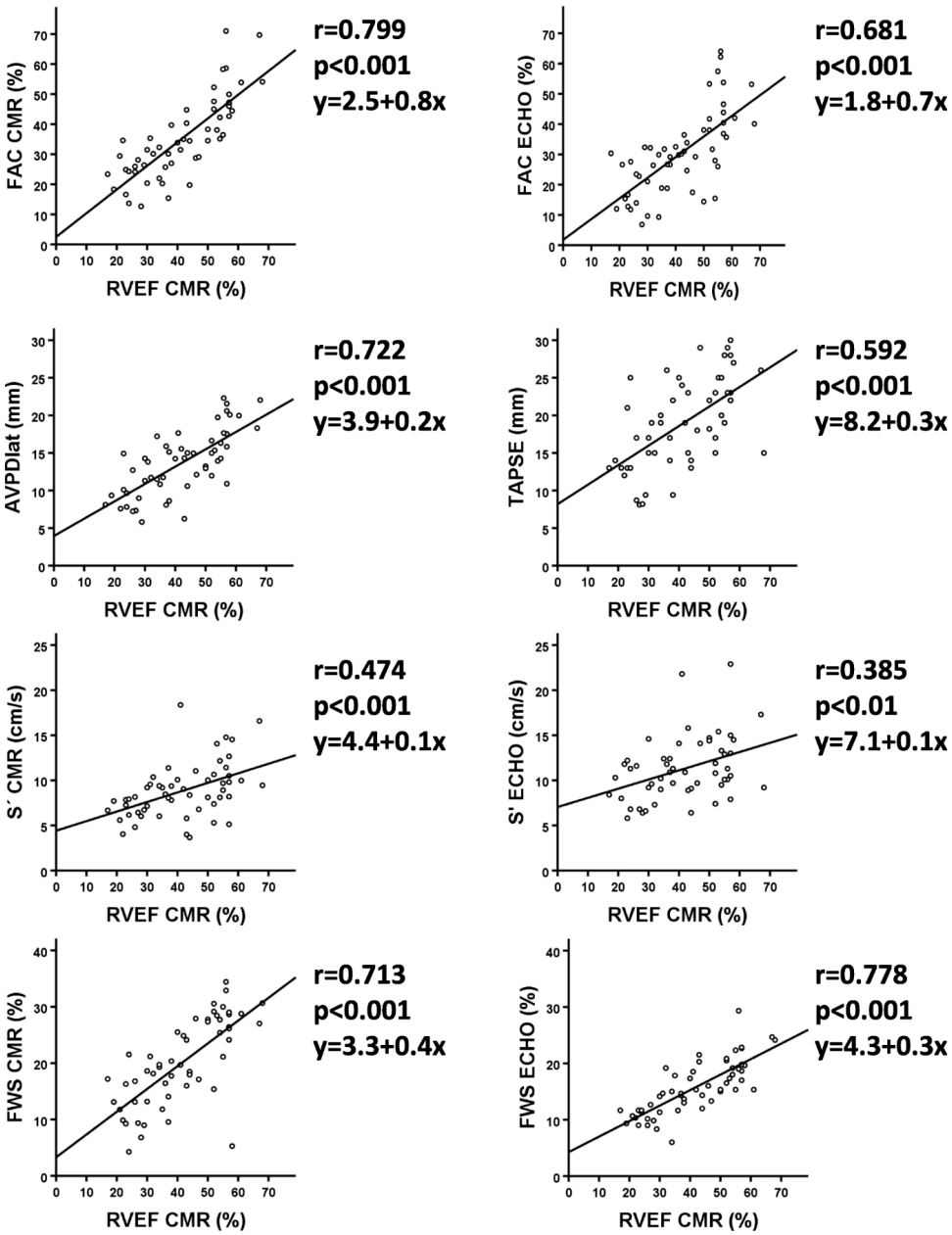

Figure 4.5: Correlation between correlation between cardiac magnetic resonance (CMR) derived parameters and corresponding echocardiographic (ECHO) derived parameters with RV ejection fraction with CMR. FAC, fractional area change; TAPSE, tricuspid annular systolic excursion; AVPDlat, lateral atrioventricular plane displacement; S', max emptying velocity; FWS, free wall strain.

4.4 Study IV

Patients with PAH had lower AVPD and longitudinal contribution to stroke volume and higher lateral contribution to stroke volume in both ventricles as well as lower septal contribution to stroke volume compared to controls (Table 4.3). Patients with lung transplantation or death had lower LV-AVPD and RV-AVPD compared to patients without lung transplantation or death (Table 4.3).

Table 4.3: Biventricular atrioventricular plane displacement (AVPD) and regional contributions to stroke volume for controls compared with patients with pulmonary arterial hypertension (PH), and patients with no death or lung transplantation compared with patients with death or lung transplantation

	Control (n = 20)	PH (n = 71)	p-value[1]	No death or tx (n = 29)	Death or tx (n = 42)	p-value[2]
Left ventricle						
LV-AVPD (mm)	16 ± 2	11 ± 3	**< 0.0001**	12 ± 3	10 ± 3	**0.02**
LV-SVlong% (%)	57 ± 8	51 ± 11	**0.02**	53 ± 11	49 ± 11	0.2
LV-SVlat% (%)	29 ± 9	48 ± 17	**< 0.0001**	45 ± 12	51 ± 19	0.1
SVsept% (%)	9 ± 4	4 ± 14	**0.01**	5 ± 12	4 ± 15	0.6
Right ventricle						
RV-AVPD (mm)	22 ± 3	12 ± 4	**< 0.0001**	13 ± 4	11 ± 3	**0.02**
RV-SVlong% (%)	85 ± 11	72 ± 19	**< 0.0001**	75 ± 20	70 ± 19	0.3
RV-SVlat% (%)	27 ± 9	34 ± 16	**0.01**	31 ± 14	36 ± 17	0.1

Death or tx, death or lung transplantation; PH, pulmonary arterialhypertension; LV, left ventricle; AVPD, atrioventricular plane displacement; SVlat%,lateral contribution to stroke volume; SVlong%, longitudinalcontribution to stroke volume; SVsept%, septal contribution tostroke volume,;RV, right ventricle. Significant values in bold. 1, control/PH; 2, no death or tx/death or tx

Patients with LV-AVPD and RV-AVPD below normal values had lower transplantation-free survival compared to patients with values within limits in Kaplan-Meier analysis (Figure. 4.6). AVPD in both ventricles were associated with decreased transplantation-free survival both in univariate and bivariate analysis (Table 4.4).

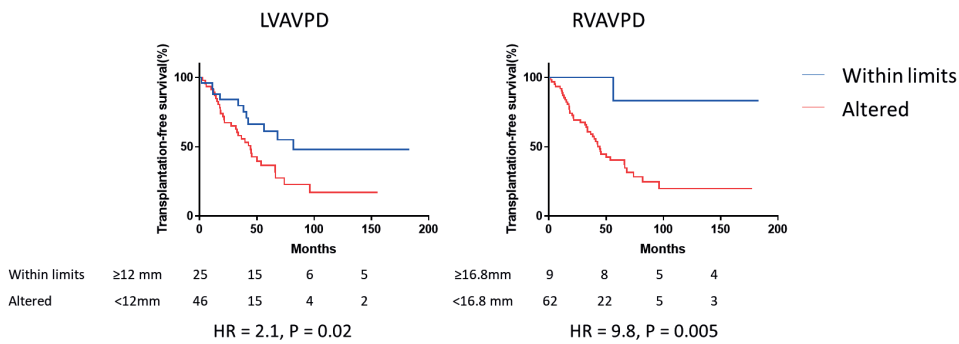

Figure 4.6: Kaplan-Meier curves for comparison of survival between patients regarding left ventricular atrioventriclar plane displacement (LVAVPD), left panel and right ventricular (RV)APPD, right panel. Blue lines depict patients with values within limits and red lines depict patients with values below limits.

Table 4.4: Univariate and bivariate (adjusted for age) cox regression analysis for transplantation-free survival.

	Univariate HR (95% CI)	**Univariate p-value**	**Bivariate[a] HR (95% CI)**	**Bivariate[a] p-value**
LV-AVPD	1.16 (1.04–1.28)	**0.007**	1.16 (1.04–1.29)	**0.008**
RV-AVPD	1.11 (1.03–1.20)	**0.01**	1.12 (1.03–1.21)	**0.01**
Age	1.03 (1.01–1.05)	**0.003**	–	–

HR hazard ratio for decrease in each incremental step, CI confidenceinterval, LV-AVPD left ventricular atrio-ventricular displacement, RV-AVPDright ventricular atrio-ventricular displacement.
a, bivariate with age.

4.5 Study V

Patients with events had higher proportion of presence of post systolic contraction (62% vs. 39%, p = 0.03) and longer time to post systolic contraction (6±8 vs. 9±9, p = 0.047) in the midventricular short axis slice compared to patients without events.
RV global longitudinal strain was associated with transplantation free survival in bivariate analysis. Dyssynchrony when including all three views, midventricular short axis stach, 4-chamber view and RV 3-chamber view, was associated with transplantation free survival in both univariate and bivariate analysis (Table 4.5).

Table 4.5: Univariate, bivariate (adjusted for age). Cox regression analysis for lung transplantation or death.

	Univariate HR (95% CI)	Univariate p-value	Bivariate[a] HR (95% CI)	Bivariate[a] p-value
RV GLS in 4ch	1.06 (0.99-1.12)	0.09	1.09 (1.02-1.18)	**0.03**
Dyssynchrony in 1 view	1.00 (0.95-1.06)	1.0		
Dyssynchrony in 2 views	1.05 (0.98-1.12)	0.2		
Dyssynchrony in 3 views	1.09 ((1.01-1.17)	**0.03**	1.1 (1.01-1.20)	**0.008**
Age	1.04 (1.02-1.05)	**<0.001**		

Univariate analysisfor increased risk of lung transplantation or death with continuous variables and bivariate analysis adjusted for age. HR, hazardratio for increase in each incremental step; CI, confidence interval; RV, rightventricular; GLS, global longitudinal strain; 4ch, 4 chamber view.

Chapter 5

5 Discussion

The main findings of this thesis have been that novel methods, such as strain, AVPD, regional contribution to stroke volume and RV dyssynchrony using CMR in PAH have diagnostic and prognostic value. In addition this thesis showed that these novel measures between echocardiography and CMR correlates but are not interchangable in PAH. Discussions on the specific findings are presented in detail in the manuscripts. The main findings of this thesis fits in a larger perspective together with a plethora of studies evaluating the utility of CMR in PAH.

It is important to arrive to a correct diagnosis in PAH, including differentiation of underlying etiologies of PH, as different etiologies have different treatment regimens. It is also important to understand the physiology behind PAH. The understanding of physiology leads to future improvements in diagnostics and treatments PAH. It is also important to arrive to the correct prognosis.

Although PAH is still a serious disorder with high mortality, there has been alot of progress during the decades. A study published in 1991 showed that mean survival in PAH was 2.8 years with 5-year survival of 34% [112]. More recent 5-year survival rate is around 60% [40–43]. This progress has been achieved by increasing the knowledge about the physiology, diagnostics and treatment of PAH. Although understanding and survival has improved it is obvious that more must be done as PAH is still a disease with high mortality.

The modality most commonly used for screening in PAH is echocardiography due to its availability and possibility of estimating pulmonary pressures [74, 75, 113]. For definite diagnosis and for differentiation between precapillary PH and postcapillary PH, RHC must be performed [114]. For further differentiation between PAH and CTEPH ventilation perfusion scans and pulmonary angiography is used [115]. Other methods of diagnosing and monitoring PAH patients are blood tests such as N-terminal pro-brain natriuretic peptide and clinical markers such as the 6-minute walk test [116, 117]. CMR is the gold standard for assessment of the RV mass, function and volumes but is still underutilized in PAH [76, 79, 118].

CMR is not new in PAH and it was shown as early as 1985 that CMR imaging of the pulmonary artery might be useful in estimating PVR non-invasively [119]. Some of the prognostic markers that have been identified in the current guidelines such as RV end diastolic volume, decreased LV end diastolic volume, decreased RVEF and decreased stroke volume are measured most accurately with CMR [18, 81]. RVEF has earlier been identified as the strongest prognostic marker in patients with PAH [120, 121]. In this thesis we explored new prognostic markers with CMR and found that AVPD in both ventricles as well as dyssynchrony from 4-chamber, short axis and RV 3-chamber views were prognostic in PAH. Currently echocardiography is the most commonly used method for non-invasively estimating pulmonary pressures [74]. In this thesis we found that strain in both the LV and the RV correlates with mPAP and pulmonary vascular resistance. There are studies that show mPAP can be estimated with CMR by assessing vortex formation in the pulmonary artery [122, 123]. There are also studies showing that CMR could aid in estimating pulmonary vascular resistance [124, 125].

In this thesis it was shown that novel methods such as lateral AVPD, tricuspid annular systolic excursion, max emptying velocity, fractional area change and RV free wall strain correlated between CMR and echocardiography in patients with PAH. But, although there were significant correlations between echocardiography and CMR they should not be used interchangeably. This could be important as echocardiography and CMR are often used as complementary modalities. Something that will probably be more common in the future. For healthy controls another study has showed that tricuspid annular plane systolic excursion and mitral annular plane systolic excursion are interchangeable between echocardiography and CMR in healthy controls [126]. This might also highlight the importance of performing studies specifically for patients with PAH, rather than referencing studies on healthy controls, when evaluating and validating new methods.

Different modalities have different advantages and disadvantages. While CMR lives up to some important requirements such as being user independent and highly reproducible it does have some disadvantages. One disadvantage is that CMR is still not available to the same degree as other modalities such as echocardiography globally [85]. Another disadvantage with CMR in PAH is that it can be difficult for patients with PAH to lie flat in with repeated breath-holds for around one hour.

To improve survival in PAH there must be more research into understanding the physiology of PAH. All modalities for assessing PAH have advantages and disadvantages and it is certain that these different modalities, including CMR, will further complement each other to improve survival and quality of life in PAH in the future.

Chapter 6

6 Conclusions

6.0.1 Study I

A decrease in LV and RV free wall global longitudinal strain is more likely associated with PAH than systemic sclerosis per se. The correlation between left and right global longitudinal strain and pulmonary arterial pressure could open possibilities for non-invasive evaluations of pulmonary arterial pressures in patients with early signs of systemic sclerosis with PAH and to select patients eligible for RHC and monitor effects of PAH therapy. This is of importance as earlier diagnosis of PAH, at a lower risk status, previously has been shown to be related to an improved survival.

6.0.2 Study II

A comprehensive biventricular myocardial deformation study with CMR feature tracking and late gadolinium enhancement reveals early subclinical cardiac involvement in cardiac asymptomatic systemic sclerosis with normal routine cardiac evaluation. CMR contributed to differentiate the patients with silent myocardial necrosis as well as identified early RV involvement. The clinical significance of CMR deformation abnormalities for outcome and treatment goals remains to be elucidated through multicenter longitudinal studies. Study III This study has demonstrated a moderate to strong correlation of regional CMR measurements to corresponding echocardiographic measures. However, biases and to some extent wide limits of agreement, exist between the modalities. Consequently, the equivalent measures are not interchangeable at least in patients with pulmonary hypertension. The echocardiographic parameter that showed best correlation with RVEFCMR was free wall strain with echocardiography. At present, fractional area change with and free wall strain with echocardiography as well as EFCMR are the preferred methods to assess and follow up RV function in patients with pulmonary hypertension. Future investigations of the CMR

right ventricular measures, beyond RVEF, are warranted.

6.0.3 Study IV

Low left and right AVPD were both associated with outcome in PAH, but regional contributions to stroke volume and EF were not. This implies that AVPD measured with CMR could be a useful tool in assessing the disease progress and risk assessment in PAH. Study V Dyssynchrony from three views were associated with outcome in PAH whereas dyssynchrony from one or two views, presence of post systolic contraction or duration of post systolic contraction were not. This implies that comprehensive dyssynchrony assessment from multiple views, including right ventricular 3 chamber view, improves prognostication in PAH.

Chapter 7

7 Future aspects

Although this thesis has shown that strain, AVPD and RV dyssynchrony have diagnostic and prognostic value in PAH it is far from being implemented in the clinic. Since PAH is a rare disorder it is hard to gather a cohort that is large enough to guide clinical decisions in single center studies. I have had the opportunity to work in a large PAH-center that has included patients with PAH since around 20 years and as such have been able to perform prognostic studies on patient populations of over 100 patients. To be able to perform larger studies there is need for multi-center studies, requiring cooperation, perhaps over the nation borders. Large multi-center studies with CMR is one future direction that is needed for greater clinical impact.

Another future direction that is currently planned is to evaluate the utility of CMR in the follow-up of PAH. I have submitted and received acceptance for an ethics application with the plan to perform rescans with CMR on patients that have already been scanned with CMR at baseline. The rescans will be done in conjunction with clinical follow-ups for PAH patients. These rescans have already started but it will take years before a large cohort has been gathered. The plan is to evaluate the utility of novel methods with CMR in follow-up and evaluation of treatment in PAH. This is something that is planned for research after the dissertation.

Bibliography

1. Rehman I, Rehman A (2022) Anatomy, Thorax, Heart

2. Shoja MM, Agutter PS, Loukas M, et al (2013) Leonardo da Vinci's studies of the heart. Int J Cardiol 167:1126–1133.

3. Anderson RH, Spicer DE, Brown NA, Mohun TJ (2014) The Development of Septation in the Four-Chambered Heart. Anat Rec 297:1414–1429.

4. Anderson RH, Brown NA (1996) The anatomy of the heart revisited. Anat Rec 246:1–7.

5. Spicer DE, Bridgeman JM, Brown NA, et al (2014) The anatomy and development of the cardiac valves. Cardiol Young 24:1008–1022.

6. Lang RM, Cameli M, Sade LE, et al (2022) Imaging assessment of the right atrium: anatomy and function. Eur Hear J - Cardiovasc Imaging 23:867–884.

7. Dell'Italia LJ (2012) Anatomy and Physiology of the Right Ventricle. Cardiol Clin 30:167–187.

8. Wagner PD (2015) The physiological basis of pulmonary gas exchange: implications for clinical interpretation of arterial blood gases. Eur Respir J 45:227–243.

9. Carpenito M, Fanti D, Mega S, et al (2021) The Central Role of Left Atrium in Heart Failure. Front Cardiovasc Med 8:.

10. Berman MN, Tupper C, Bhardwaj A (2022) Physiology, Left Ventricular Function

11. Sacks MS, Yoganathan AP (2007) Heart valve function: a biomechanical perspective. Philos Trans R Soc B Biol Sci 362:1369–1391.

12. Nagueh SF (2020) Left Ventricular Diastolic Function. JACC Cardiovasc Imaging 13:228–244.

13. Little WC, Downes TR (1990) Clinical evaluation of left ventricular diastolic performance. Prog Cardiovasc Dis 32:273–290.

14. WALLACE AG, MITCHELL JH, SKINNER NS, SARNOFF SJ (1963) Duration of the Phases of Left Ventricular Systole. Circ Res 12:611–619.

15. ADELMAN AG, WIGLE ED (1968) Two Types of Intraventricular Pressure Difference in the Same Patient. Circulation 38:649–655.

16. Buechel EV, Kaiser T, Jackson C, et al (2009) Normal right- and left ventricular volumes and myocardial mass in children measured by steady state free precession cardiovascular magnetic resonance. J Cardiovasc Magn Reson 11:19.

17. Kawel-Boehm N, Maceira A, Valsangiacomo-Buechel ER, et al (2015) Normal values for cardiovascular magnetic resonance in adults and children. J Cardiovasc Magn Reson 17:1–33.

18. Galiè N, Humbert M, Vachiery J-L, et al (2016) 2015 ESC/ERS Guidelines for the diagnosis and treatment of pulmonary hypertension. Eur Heart J 37:67–119.

19. Simonneau G, Montani D, Celermajer DS, et al (2019) Haemodynamic definitions and updated clinical classification of pulmonary hypertension. Eur Respir J 53:1801913.

20. Hoeper MM, Humbert M (2019) The new haemodynamic definition of pulmonary hypertension: evidence prevails, finally! Eur Respir J 53:1900038.

21. Nagy AI, Venkateshvaran A, Dash PK, et al (2014) The pulmonary capillary wedge pressure accurately reflects both normal and elevated left atrial pressure. Am Heart J 167:876–883.

22. Guignabert C, Dorfmuller P (2013) Pathology and Pathobiology of Pulmonary Hypertension. Semin Respir Crit Care Med 34:551–559.

23. Shimoda LA, Laurie SS (2013) Vascular remodeling in pulmonary hypertension. J Mol Med 91:297–309.

24. Davie N, Haleen SJ, Upton PD, et al (2002) ET A and ET B Receptors Modulate the Proliferation of Human Pulmonary Artery Smooth Muscle Cells. Am J Respir Crit Care Med 165:398–405.

25. Cao Y, Geng C, Li Y, Zhang Y (2021) In situ Pulmonary Artery Thrombosis: A Previously Overlooked Disease. Front Pharmacol 12:.

26. Oka M, Homma N, Taraseviciene-Stewart L, et al (2007) Rho Kinase–Mediated Vasoconstriction Is Important in Severe Occlusive Pulmonary Arterial Hypertension in Rats. Circ Res 100:923–929.

27. Tuder RM, Archer SL, Dorfmüller P, et al (2013) Relevant Issues in the Pathology and Pathobiology of Pulmonary Hypertension. J Am Coll Cardiol 62:D4–D12.

28. Christman BW, McPherson CD, Newman JH, et al (1992) An Imbalance between the Excretion of Thromboxane and Prostacyclin Metabolites in Pulmonary Hypertension. N Engl J Med 327:70–75.

29. Rubin LJ, Badesch DB, Barst RJ, et al (2002) Bosentan Therapy for Pulmonary Arterial Hypertension. N Engl J Med 346:896–903.

30. Lázár Z, Mészáros M, Bikov A (2020) The Nitric Oxide Pathway in Pulmonary Arterial Hypertension: Pathomechanism, Biomarkers and Drug Targets. Curr Med Chem 27:7168–7188.

31. Del Pozo R, Hernandez Gonzalez I, Escribano-Subias P (2017) The prostacyclin pathway in pulmonary arterial hypertension: a clinical review. Expert Rev Respir Med 11:491–503.

32. Vonk Noordegraaf A, Westerhof BE, Westerhof N (2017) The Relationship Between the Right Ventricle and its Load in Pulmonary Hypertension. J Am Coll Cardiol 69:236–243.

33. Lai YC, Potoka KC, Champion HC, et al (2014) Pulmonary arterial hypertension: the clinical syndrome. Circ Res 115:115–130.

34. Galié N, Manes A, Palazzini M, et al (2007) Pharmacological impact on right ventricular remodelling in pulmonary arterial hypertension. Eur Hear J Suppl 9:H68–H74.

35. Ivarsson B, Johansson A, Kjellström B (2021) The Odyssey from Symptom to Diagnosis of Pulmonary Hypertension from the Patients and Spouses Perspective. J Prim Care Community Health 12:215013272110292.

36. Khou V, Anderson JJ, Strange G, et al (2020) Diagnostic delay in pulmonary arterial hypertension: Insights from the Australian and New Zealand pulmonary hypertension registry. Respirology 25:863–871.

37. Strange G, Gabbay E, Kermeen F, et al (2013) Time from Symptoms to Definitive Diagnosis of Idiopathic Pulmonary Arterial Hypertension: The Delay Study. Pulm Circ 3:89–94.

38. Peacock a J, Murphy NF, McMurray JJ V, et al (2007) An epidemiological study of pulmonary arterial hypertension. Eur Respir J Off J Eur Soc Clin Respir Physiol 30:104–109.

39. Rådegran G, Kjellström B, Ekmehag B, et al (2016) Characteristics and survival of adult Swedish PAH and CTEPH patients 2000–2014. Scand Cardiovasc J 50:243–250.

40. Korsholm K, Andersen A, Kirkfeldt RE, et al (2015) Survival in an incident cohort of patients with pulmonary arterial hypertension in Denmark. Pulm Circ 5:364–369.

41. Benza RL, Miller DP, Barst RJ, et al (2012) An evaluation of long-term survival from time of diagnosis in pulmonary arterial hypertension from the reveal registry. Chest 142:448–456.

42. Humbert M, Sitbon O, Yaïci a., et al (2010) Survival in incident and prevalent cohorts of patients with pulmonary arterial hypertension. Eur Respir J 36:549–555.

43. Thenappan T, Shah SJ, Rich S, et al (2010) Survival in pulmonary arterial hypertension: A reappraisal of the NIH risk stratification equation. Eur Respir J 35:1079–1087.

44. Kawut S m., Taichman DB, Archer-Chicko CL, et al (2003) Hemodynamics and survival in patients with pulmonary arterial hypertension related to systemic sclerosis. Chest 123:344–50

45. Hjalmarsson C, Kjellström B, Jansson K, et al (2021) Early risk prediction in idiopathic versus connective tissue disease-associated pulmonary arterial hypertension: call for a refined assessment. ERJ Open Res 7:00854–02020.

46. Kylhammar D, Hjalmarsson C, Hesselstrand R, et al (2021) Predicting mortality during long-term follow-up in pulmonary arterial hypertension. ERJ Open Res 7:00837–02020.

47. Wilkins MR, Wharton J, Grimminger F, Ghofrani HA (2008) Phosphodiesterase inhibitors for the treatment of pulmonary hypertension. Eur Respir J 32:198–209.

48. Stasch J-P, Pacher P, Evgenov O V. (2011) Soluble Guanylate Cyclase as an Emerging Therapeutic Target in Cardiopulmonary Disease. Circulation 123:2263–2273.

49. Sood N, Aranda A, Platt D, et al (2018) Riociguat improves health-related quality of life for patients with pulmonary arterial hypertension: results from the phase 4 MOTION study. Pulm Circ 9:3–9.

50. Stuart R, Elizabeth K, paul s. L (1992) The Effect of High Doses of Calcium-Channel Blockers on Survival in Primary Pulmonary Hypertension. N Engl J Med 76–81

51. Gaine S, McLaughlin V (2017) Pulmonary arterial hypertension: tailoring treatment to risk in the current era. Eur Respir Rev 26:170095.

52. Rubio-Rivas M, Royo C, Simeón CP, et al (2014) Mortality and survival in systemic sclerosis: Systematic review and meta-analysis. Semin Arthritis Rheum 44:208–219.

53. Lefèvre G, Dauchet L, Hachulla E, et al (2013) Survival and prognostic factors in systemic sclerosis-associated pulmonary hypertension: A systematic review and meta-analysis. Arthritis Rheum 65:2412–2423.

54. Roberts-Thomson PJ, Jones M, Hakendorf P, et al (2001) Scleroderma in South Australia: epidemiological observations of possible pathogenic significance. Intern Med J 31:220–229.

55. Mayes MD, Lacey J V., Beebe-Dimmer J, et al (2003) Prevalence, incidence, survival, and disease characteristics of systemic sclerosis in a large US population. Arthritis Rheum 48:2246–2255.

56. Arias-Nuñez MC, Llorca J, Vazquez-Rodriguez TR, et al (2008) Systemic Sclerosis in Northwestern Spain. Medicine (Baltimore) 87:272–280.

57. van den Hoogen F, Khanna D, Fransen J, et al (2013) 2013 Classification Criteria for Systemic Sclerosis: An American College of Rheumatology/European League Against Rheumatism Collaborative Initiative. Arthritis Rheum 65:2737–2747.

58. McLaughlin V V., Archer SL, Badesch DB, et al (2009) ACCF/AHA 2009 Expert Consensus Document on Pulmonary Hypertension. A Report of the American College of Cardiology Foundation Task Force on Expert Consensus Documents and the American Heart Association Developed in Collaboration With the American College o. J. Am. Coll. Cardiol.

59. Krishnan A, Markham R, Savage M, et al (2019) Right Heart Catheterisation: How To Do It. Hear Lung Circ 28:e71–e78.

60. Swan HJC, Ganz W, Forrester J, et al (1970) Catheterization of the Heart in Man with Use of a Flow-Directed Balloon-Tipped Catheter. N Engl J Med 283:447–451.

61. Hoeper MM, Lee SH, Voswinckel R, et al (2006) Complications of Right Heart Catheterization Procedures in Patients With Pulmonary Hypertension in Experienced Centers. J Am Coll Cardiol 48:2546–2552.

62. Shah S, Boyd G, Pyne CT, et al (2014) Right heart catheterization using antecubital venous access: Feasibility, safety and adoption rate in a tertiary center. Catheter Cardiovasc Interv 84:70–74.

63. Roule V, Ailem S, Legallois D, et al (2015) Antecubital vs Femoral Venous Access for Right Heart Catheterization: Benefits of a Flashback. Can J Cardiol 31:1497.e1-1497.e6.

64. Ranu H, Smith K, Nimako K, et al (2010) A Retrospective Review to Evaluate the Safety of Right Heart Catheterization via the Internal Jugular Vein in the Assessment of Pulmonary Hypertension. Clin Cardiol 33:303–306.

65. Leibowitz A, Oren-Grinberg A, Matyal R (2020) Ultrasound Guidance for Central Venous Access: Current Evidence and Clinical Recommendations. J Intensive Care Med 35:303–321.

66. Ganz W, Swan HJC (1972) Measurement of blood flow by thermodilution. Am J Cardiol 29:241–246.

67. Augustine DX, Coates-Bradshaw LD, Willis J, et al (2018) Echocardiographic assessment of pulmonary hypertension: a guideline protocol from the British Society of Echocardiography. Echo Res Pract 5:G11–G24.

68. Mitchell C, Rahko PS, Blauwet LA, et al (2019) Guidelines for Performing a Comprehensive Transthoracic Echocardiographic Examination in Adults: Recommendations from the American Society of Echocardiography. J Am Soc Echocardiogr 32:1–64.

69. Zhou Q, Lam KH, Zheng H, et al (2014) Piezoelectric single crystal ultrasonic transducers for biomedical applications. Prog Mater Sci 66:87–111.

70. Edler I, Hertz CH (2004) The Use of Ultrasonic Reflectoscope for the Continuous Recording of the Movements of Heart Walls. Clin Physiol Funct Imaging 24:118–136.

71. Feigenbaum H (2010) Role of M-mode Technique in Today's Echocardiography. J Am Soc Echocardiogr 23:240–257.

72. Holen J, Simonsen S (1979) Determination of pressure gradient in mitral stenosis with Doppler echocardiography. Heart 41:529–535.

73. Hatle L, Angelsen BA, Tromsdal A (1980) Non-invasive assessment of aortic stenosis by Doppler ultrasound. Heart 43:284–292.

74. Yock PG, Popp RL (1984) Noninvasive estimation of right ventricular systolic pressure by Doppler ultrasound in patients with tricuspid regurgitation. Circulation 70:657–662

75. Currie PJ, Seward JB, Chan K, et al (1985) Continuous Wave Doppler Determination of Right Ventricular Pressure: A Simultaneous Doppler-Catheterization Study in 127 Patients. J Am Coll Cardiol 6:750–756.

76. Benza R, Biederman R, Murali S, Gupta H (2008) Role of Cardiac Magnetic Resonance Imaging in the Management of Patients With Pulmonary Arterial Hypertension. J Am Coll Cardiol 52:1683–1692.

77. Rudski LG, Lai WW, Afilalo J, et al (2010) Guidelines for the Echocardiographic Assessment of the Right Heart in Adults: A Report from the American Society of Echocardiography Endorsed by the European Association of Echocardiography , a registered branch of the European Society of Cardiology , an. J Am Soc Echocardiogr 23:685–713.

78. Lang RM, Badano LP, Mor-Avi V, et al (2015) Recommendations for cardiac chamber quantification by echocardiography in adults: An update from the American society of echocardiography and the European association of cardiovascular imaging. Eur Heart J Cardiovasc Imaging 16:233–271.

79. Sugeng L, Mor-Avi V, Weinert L, et al (2010) Multimodality Comparison of Quantitative Volumetric Analysis of the Right Ventricle. JACC Cardiovasc Imaging 3:10–18.

80. van de Veerdonk MC, Kind T, Marcus JT, et al (2011) Progressive Right Ventricular Dysfunction in Patients With Pulmonary Arterial Hypertension Responding to Therapy. J Am Coll Cardiol 58:2511–2519.

81. van Wolferen SA, Marcus JT, Boonstra A, et al (2007) Prognostic value of right ventricular mass, volume, and function in idiopathic pulmonary arterial hypertension. Eur Heart J 28:1250–1257.

82. Yamada Y, Okuda S, Kataoka M, et al (2012) Prognostic Value of Cardiac Magnetic Resonance Imaging for Idiopathic Pulmonary Arterial Hypertension Before Initiating Intravenous Prostacyclin Therapy. Circ J 76:1737–1743.

83. Swift AJ, Rajaram S, Campbell MJ, et al (2014) Prognostic value of cardiovascular

magnetic resonance imaging measurements corrected for age and sex in idiopathic pulmonary arterial hypertension. Circ Cardiovasc Imaging 7:100–106.

84. Kjellström B, Lindholm A, Ostenfeld E (2020) Cardiac Magnetic Resonance Imaging in Pulmonary Arterial Hypertension: Ready for Clinical Practice and Guidelines? Curr Heart Fail Rep 17:181–191.

85. The OECD. (2020) Health equipment — Magnetic resonance imaging (MRI) units — OECD Data. http://data.oecd.org/healtheqt/magnetic-resonance-imaging-mri-units.htm

86. Serai SD, Ho M-L, Artunduaga M, et al (2021) Components of a magnetic resonance imaging system and their relationship to safety and image quality. Pediatr Radiol 51:716–723.

87. Gruber B, Froeling M, Leiner T, Klomp DWJ (2018) RF coils: A practical guide for nonphysicists. J Magn Reson Imaging 48:590–604.

88. Hidalgo-Tobon SS (2010) Theory of gradient coil design methods for magnetic resonance imaging. Concepts Magn Reson Part A 36A:223–242.

89. McVeigh ER, Bronskill MJ, Henkelman RM (1986) Phase and sensitivity of receiver coils in magnetic resonance imaging. Med Phys 13:806–814.

90. Popkin BM, D'Anci KE, Rosenberg IH (2010) Water, hydration, and health. Nutr Rev 68:439–458.

91. Fraser RGJ (1927) The effective cross section of the oriented hydrogen atom. Proc R Soc London Ser A, Contain Pap a Math Phys Character 114:212–221.

92. Pai A, Shetty R, Chowdhury YS (2022) Magnetic Resonance Imaging Physics

93. Lee JH, Okuno Y, Cavagnero S (2014) Sensitivity enhancement in solution NMR: Emerging ideas and new frontiers. J Magn Reson 241:18–31.

94. Larmor J (1897) IX. A dynamical theory of the electric and luminiferous medium.—Part III. relations with material media. Philos Trans R Soc London Ser A, Contain Pap a Math or Phys Character 190:205–300.

95. Støylen A, Mølmen HE, Dalen H (2019) Left ventricular global strains by linear measurements in three dimensions: interrelations and relations to age, gender and body size in the HUNT Study. Open Hear 6:e001050.

96. Greenbaum RA, Ho SY, Gibson DG, et al (1981) Left ventricular fibre architecture in man. Heart 45:248–263.

97. Streeter DD, Spotnitz HM, Patel DP, et al (1969) Fiber Orientation in the Canine Left Ventricle during Diastole and Systole. Circ Res 24:339–347.

98. Buckberg G, Hoffman JIE (2014) Right ventricular architecture responsible for mechanical performance: Unifying role of ventricular septum. J Thorac Cardiovasc Surg 148:3166-3171.e4.

99. Carlsson M, Ugander M, Heiberg E, Arheden H (2007) The quantitative relationship between longitudinal and radial function in left, right, and total heart pumping in humans. Am J Physiol Circ Physiol 293:H636–H644.

100. Willenheimer R, Cline C, Erhardt L, Israelsson B (1997) Left ventricular atrioventricular plane displacement: an echocardiographic technique for rapid assessment of prognosis in heart failure. Heart 78:230–236.

101. Rydberg E, Arlbrandt M, Gudmundsson P, et al (2003) Left atrioventricular plane displacement predicts cardiac mortality in patients with chronic atrial fibrillation. Int J Cardiol 91:1–7.

102. Svealv BG, Olofsson EL, Andersson B (2008) Ventricular long-axis function is of major importance for long-term survival in patients with heart failure. Heart 94:284–289.

103. Ostenfeld E, Stephensen SS, Steding-Ehrenborg K, et al (2016) Regional contribution to ventricular stroke volume is affected on the left side, but not on the right in patients with pulmonary hypertension. Int J Cardiovasc Imaging 2016 Aug;3:1243–53.

104. Lindholm A, Kjellström B, Seemann F, et al (2022) Atrioventricular plane displacement and regional function to predict outcome in pulmonary arterial hypertension. Int J Cardiovasc Imaging.

105. Steding K, Engblom H, Buhre T, et al (2010) Relation between cardiac dimensions and peak oxygen uptake. J Cardiovasc Magn Reson 12:8.

106. Bodetoft S, Carlsson M, Arheden H, Ekelund U (2011) Effects of oxygen inhalation on cardiac output , coronary blood flow and oxygen delivery in healthy individuals , assessed with MRI. Eur J Emerg Med 18:25–30.

107. Gyllenhammar T, Kanski M, Engblom H, et al (2018) Decreased global myocardial perfusion at adenosine stress as a potential new biomarker for microvascular disease in systemic sclerosis : a magnetic resonance study. BMC Cardiovasc Disord 18:1–8.

108. Lang RM, Badano LP, Mor-Avi V, et al (2015) Recommendations for Cardiac Chamber Quantification by Echocardiography in Adults: An Update from the American Society of Echocardiography and the European Association of Cardiovascular Imaging. J Am Soc Echocardiogr 28:1-39.e14.

109. Evaldsson AW, Lindholm A, Jumatate R, et al (2020) Right ventricular function parameters in pulmonary hypertension: Echocardiography vs. cardiac magnetic resonance. BMC Cardiovasc Disord 20:1–12.

110. Heiberg E, Sjögren J, Ugander M, et al (2010) Design and validation of Segment - freely available software for cardiovascular image analysis. BMC Med Imaging 10:1.

111. Froud R, Abel G (2014) Using ROC curves to choose minimally important change thresholds when sensitivity and specificity are valued equally: The forgotten lesson of pythagoras. Theoretical considerations and an example application of change in health status. PLoS One 9:1–11.

112. D'Alonzo GE (1991) Survival in Patients with Primary Pulmonary Hypertension. Ann Intern Med 115:343.

113. Jang AY, Shin M-S (2020) Echocardiographic Screening Methods for Pulmonary Hypertension: A Practical Review. J Cardiovasc Imaging 28:1.

114. Galie N, Hoeper MM, Humbert M, et al (2009) Guidelines for the diagnosis and treatment of pulmonary hypertension: The Task Force for the Diagnosis and Treatment of Pulmonary Hypertension of the European Society of Cardiology (ESC) and the European Respiratory Society (ERS), endorsed by the Internat. Eur Heart J.

115. Memon HA, Lin CH, Guha A (2016) Chronic Thromboembolic Pulmonary Hypertension: Pearls and Pitfalls of Diagnosis. Methodist Debakey Cardiovasc J 12:199.

116. Berghaus TM, Kutsch J, Faul C, et al (2017) The association of N-terminal pro-brain-type natriuretic peptide with hemodynamics and functional capacity in therapy-naive precapillary pulmonary hypertension: results from a cohort study. BMC Pulm Med 17:167.

117. Deboeck G (2005) Physiological response to the six-minute walk test in pulmonary arterial hypertension. Eur Respir J 26:667–672.

118. Boxt LM, Katz J (1993) Magnetic Resonance Imaging for Quantitation of Right Ventricular Volume in Patients with Pulmonary Hypertension. J Thorac Imaging 8:92–97.

119. von SCHULTHESS GK (1985) Pathologic Blood Flow in Pulmonary Vascular Disease as Shown by Gated Magnetic Resonance Imaging. Ann Intern Med 103:317.

120. Baggen VJM, Leiner T, Post MC, et al (2016) Cardiac magnetic resonance findings predicting mortality in patients with pulmonary arterial hypertension: a systematic review and meta-analysis. Eur Radiol 26:3771–3780.

121. Dong Y, Pan Z, Wang D, et al (2020) Prognostic Value of Cardiac Magnetic Resonance-Derived Right Ventricular Remodeling Parameters in Pulmonary Hypertension: A Systematic Review and Meta-Analysis. Circ Cardiovasc Imaging 13:1–12.

122. Ramos JG, Fyrdahl A, Wieslander B, et al (2020) Cardiovascular magnetic resonance 4D flow analysis has a higher diagnostic yield than Doppler echocardiography for detecting increased pulmonary artery pressure. BMC Med Imaging 20:28.

123. Reiter U, Reiter G, Kovacs G, et al (2013) Evaluation of elevated mean pulmonary arterial pressure based on magnetic resonance 4D velocity mapping: Comparison of visualization techniques. PLoS One 8:1–9.

124. Garcia-Alvarez A, Fernandez-Friera L, Mirelis JG, et al (2011) Non-invasive estimation of pulmonary vascular resistance with cardiac magnetic resonance. Eur Heart J 32:2438–2445.

125. Bane O, Shah SJ, Cuttica MJ, et al (2015) A non-invasive assessment of cardiopulmonary hemodynamics with MRI in pulmonary hypertension. Magn Reson Imaging 33:1224–1235.

126. Sepúlveda-Martínez A, Steding-Ehrenborg K, Rodríguez-López M, et al (2021) Atrioventricular plane displacement versus mitral and tricuspid annular plane systolic excursion: a comparison between cardiac magnetic resonance and M□mode echocardiography. Clin Physiol Funct Imaging 0–3.

Where is everybody?
- Enrico Fermi